© 2017. Published by The Company of Biologists Ltd | Journal of Cell Science (2017) 130, 2416-2429 doi:10.1242/jcs.195875

RESEARCH ARTICLE

Reconstitution of the oocyte nucleolus in mice through a single nucleolar protein, NPM2

Sugako Ogushi[1,2,*,‡], Kazuo Yamagata[3], Chikashi Obuse[4], Keiko Furuta[5], Teruhiko Wakayama[3], Martin M. Matzuk[6] and Mitinori Saitou[2,7,8,9]

ABSTRACT

The mammalian oocyte nucleolus, the most prominent subcellular organelle in the oocyte, is vital in early development, yet its key functions and constituents remain unclear. We show here that the parthenotes/zygotes derived from enucleolated oocytes exhibited abnormal heterochromatin formation around parental pericentromeric DNAs, which led to a significant mitotic delay and frequent chromosome mis-segregation upon the first mitotic division. A proteomic analysis identified nucleoplasmin 2 (NPM2) as a dominant component of the oocyte nucleolus. Consistently, *Npm2*-deficient oocytes, which lack a normal nucleolar structure, showed chromosome segregation defects similar to those in enucleolated oocytes, suggesting that nucleolar loss, rather than micromanipulation-related damage to the genome, leads to a disorganization of higher-order chromatin structure in pronuclei and frequent chromosome mis-segregation during the first mitosis. Strikingly, expression of NPM2 alone sufficed to reconstitute the nucleolar structure in enucleolated embryos, and rescued their first mitotic division and full-term development. The nucleolus rescue through NPM2 required the pentamer formation and both the N- and C-terminal domains. Our findings demonstrate that the NPM2-based oocyte nucleolus is an essential platform for parental chromatin organization in early embryonic development.

KEY WORDS: Oocyte, Nucleolus, Heterochromatin, Nucleoplasmin 2

INTRODUCTION

In multicellular organisms, germ cells are the only cells that carry genetic information from one generation to the next. During germ cell formation, reprogramming of chromatin occurs to reset the parental epigenetic memory for the creation of new individuals (Saitou et al., 2012). Not only chromatin but also cellular organelles, such as centrosomes and mitochondria, transform their morphology; however, the significance and the mechanism of organelle transformation during gametogenesis are not well-understood (Sutovsky and Schatten, 1998). As gametogenesis reaches the final phase, the nucleolus transforms into a highly compact and fibrillar structure in oocytes and lacks rDNA transcription (Chouinard, 1971). After fertilization, the morphology of the nucleolus gradually changes from an oocyte type to a somatic one, accompanied by the development of active rDNA transcription as early embryonic development proceeds (Geuskens and Alexandre, 1984).

The nucleolus is the largest sub-nuclear structure and is generally considered the site for ribosome biogenesis. However, because the oocyte nucleolus does not exhibit transcription of rRNA, it had been regarded as a remnant of the nucleolus structure during oogenesis or a precursor of the nucleolus for early embryonic development. The first clear clue in regard to the oocyte nucleolus function came from *Npm2*-knockout experiments, which showed that *Npm2*-deficient oocytes lacked the nucleolus and were unable to proceed with the correct development in mice (Burns et al., 2003). In amphibians, nucleoplasmin/NPM2 has been shown to have a dual function – i.e. acting as a histone chaperone by binding to histone H2A-H2B (Kleinschmidt et al., 1985; Laskey et al., 1978) and also as an exchanger of sperm-specific basic proteins, such as protamine in mammals, for maternal histones H2A-H2B to promote sperm chromatin decondensation (Ohsumi and Katagiri, 1991; Philpott and Leno, 1992; Philpott et al., 1991). In mice, however, protamine removal and sperm chromatin decondensation occur independently of maternal histone deposition (Inoue and Zhang, 2014) and *Npm2*-null zygotes have been shown to form an apparently normal paternal pronucleus (Burns et al., 2003). Thus, in mammals, the role of NPM2 in sperm chromatin decondensation remains a mystery. Moreover, the molecular mechanisms of NPM2 in oocyte nucleolus formation are still largely unknown.

To examine the role of the oocyte nucleolus more directly, we previously have generated mouse oocytes that lack the nucleolus by using micromanipulation in a process called enucleolation (Ogushi et al., 2008). Embryos derived from enucleolated oocytes were able to synthesize proteins and to replicate DNA but failed to develop past the first few cleavages, suggesting that the oocyte nucleolus has pivotal functions that are little related to ribosome biogenesis in early embryonic development (Ogushi et al., 2008). Moreover, the critical time point, when the nucleolus is required for early embryonic development, appears to be at the early step of pronucleus formation (Kyogoku et al., 2014; Ogushi and Saitou, 2010). Zygotes from enucleolated mouse oocytes have been shown to exhibit mis-localization of centromeric proteins (Ogushi and Saitou, 2010), delay in enlargement of the paternal pronucleus (Inoue et al., 2011), alteration of DNA replication timing and abnormal deposition of fas death-domain-associated protein

[1]The Hakubi Center for Advanced Research, Kyoto University, Sakyo-ku, Kyoto 606-8501, Japan. [2]Department of Anatomy and Cell Biology, Graduate School of Medicine, Kyoto 606-8501, Japan. [3]Laboratory for Genomic Reprogramming, RIKEN Center for Developmental Biology, 2-2-3 Minatojima-Minamimachi, Chuo-ku, Kobe 650-0047, Japan. [4]Graduate School of Life Science, Hokkaido University, Sapporo, Hokkaido 001-0021, Japan. [5]Division of Electron Microscopic Study, Center for Anatomical Studies, Graduate School of Medicine, Kyoto University, Sakyo-ku, Kyoto 606-8501, Japan. [6]Departments of Pathology & Immunology, Molecular and Cellular Biology, Molecular and Human Genetics, and Pharmacology, and Center for Drug Discovery, Baylor College of Medicine, Houston, Texas 77030, USA. [7]Institute for Integrated Cell-Material Sciences, Kyoto University Institute for Advanced Study, Sakyo-ku, Kyoto 606-8501, Japan. [8]JST, CREST/ERATO, Kyoto University, Sakyo-ku, Kyoto 606-8501, Japan. [9]Department of Reprogramming Science, Center for iPS Cell Research and Application, Kyoto University, Sakyo-ku, Kyoto 606-8507, Japan.
*Present address: Department of Biochemistry, University of Oxford, South Parks Road, Oxford OX1 3QU, UK

‡Author for correspondence (sugako.ogushi@bioch.ox.ac.uk)

S.O., 0000-0001-8497-6972

Received 8 August 2016; Accepted 31 May 2017

Journal of Cell Science

Journal of Cell Science (2017) 130, 2416-2429 doi:10.1242/jcs.195875

(DAXX), a histone H3.3 chaperone protein for repetitive regions of the genome (Fulka and Langerova, 2014; Voon and Wong, 2016). In mouse *Npm2*-null zygotes, hypo-acetylated histone H3 on the heterochromatin surrounding nucleoli is lost (Burns et al., 2003). Moreover, both zygotes from enucleolated and *Npm2*-null oocytes show abnormal mitosis exit (Burns et al., 2003; Fulka and Langerova, 2014; Ogushi and Saitou, 2010). However, it is unknown which of those defects described above directly cause the developmental arrest in embryos from enucleolated oocytes and what functions and components in the oocyte nucleolus are required for early-embryonic development.

To better understand these issues, we here analyze the detailed progression of the first cell cycle in parthenotes (i.e. embryos derived from unfertilized oocytes through parthenogenetic activation rather than sperm entry) or zygotes from enucleolated and *Npm2*-null oocytes by using a combination of immunocytochemistry and live-cell imaging, and show that, in mice, the absence of a nucleolus in oocytes leads to destabilization of the chromatin at centromeric and/or pericentromeric regions and, consequently, to delay of mitosis and chromosome mis-segregation. Moreover, we show by using proteomics analysis that NPM2 is the main component of the oocyte nucleolus, and protein expression of NPM2 alone rescues the defects in early embryonic development caused by enucleolation.

RESULTS

The nucleolus is essential for centromeric/pericentromeric chromatin organization during the first mitosis

The oocyte nucleolus in a zygote might play a key role in chromatin organization because it is surrounded by pericentromeric heterochromatin (Ogushi and Saitou, 2010). To determine the physiological relevance of heterochromatin anchoring to the nucleolus, we performed enucleolation (Ogushi et al., 2008) and then examined its impact on chromatin organization in parthenotes or zygotes by using antibodies against histone H3 tri-methylated at lysine 9 (H3K9me3), which marks maternal chromatin (Arney et al., 2002) and pericentromeric heterochromatin (Probst et al., 2007), and CREST (calcinosis, Raynaud's phenomenon, esophageal dysmotility, sclerodactyly, telangiectasia) autoimmune serum which labels mouse centromeres (Broccoli et al., 1990). For whole-DNA staining, 4′,6-diamidino-2-phenylindole, dihydrochloride (DAPI) was used. Examination of the chromatin configuration in the parthenotes from enucleolated oocytes allowed us to identify any potential influence of enucleolation on paternal chromatin decondensation in the zygotes (Inoue et al., 2011).

Enucleolated oocytes that had been injected again with a nucleolus served as a control. In control parthenotes/zygotes, the intensely DAPI-positive heterochromatin was anchored to the nucleoli and formed a ring-like structure, whereas in parthenotes/zygotes from enucleolated oocytes the foci that formed were similar to chromocenters. The latter are usually observed in interphase nuclei of somatic cells but never occur in embryos before transcriptional activation of the embryonic genome (Fig. 1A and Fig. S1A) (Probst et al., 2010). Chromocenter-like foci in pronuclei from enucleolated oocytes were always strongly stained for H3K9me3, indicating pericentromeric heterochromatin. Moreover, there were one or two atypical diffuse CREST signals (>2.0 μm^2) in pronuclei of both parthenotes and zygotes from enucleolated oocytes (Fig. 1A,B and Fig. S1A,B). This indicates that centromere proteins detected by CREST serum, such as CENP-A, -B and -C, were mis-loaded onto chromatin. The number of CREST-positive foci was not significantly different from that in control oocytes, although the numbers in enucleolated parthenotes/zygotes were more divergent (Fig. 1C and Fig. S1C). This result suggests that centromere clustering, which is important for the spatial genome organization and gene expression (Tjong et al., 2016; Wijchers et al., 2015), was slightly aborted in parthenotes/zygotes from enucleolated oocytes. Therefore, the lack of nucleoli in pronuclei resulted in a disorganization of chromatin architecture establishment at centromeric/pericentromeric regions. Since we observed similar defects both in parthenotes and in zygotes from enucleolated oocytes, these defects were not caused by an abnormality of sperm chromatin decondensation.

The nucleolus is essential for correct chromosome segregation during first mitosis

The centromeric/pericentromeric chromatin is an essential region of DNA for the kinetochore assembly during mitosis (Fukagawa and Earnshaw, 2014). We, therefore, observed the progression through the first mitosis in parthenotes/zygotes from enucleolated oocytes in live-cell imaging by using mRNAs of histone *H2b* fused to *mCherry* (*H2b-mCherry*) as a chromosome marker and by using antibodies against histone H3 phosphorylation at S10 conjugated to Alexa-Fluor-488 (Fab311-Alexa488) as a chromosome condensation marker (Hayashi-Takanaka et al., 2009). Parthenotes from enucleolated oocytes showed a delayed entry into mitosis (1085±195 min) compared to those from control oocytes (933±74 min), but exhibited similar kinetics of histone H3 phosphorylation at S10 to that in the control group (Fig. 1D,E and Table S1). Eighty-three percent (15/18) of them showed delayed anaphase onset and underwent cell division with lagging chromosomes, resulting in 2-cell embryos with micronuclei. The total length of the first mitosis in parthenotes from enucleolated oocytes was 236±91 min, versus 177±43 min in the control oocytes (Fig. 1E and Table S1). Zygotes from enucleolated oocytes also exhibited a delayed entry into mitosis, which is consistent with the previous report (Fulka and Langerova, 2014), and longer duration of the first mitosis with lagging chromosomes but to a more-severe degree compared to the parthenotes from enucleolated oocytes (Fig. S1E,F and Table S1). The number of the chromosomes in parthenotes/zygotes from enucleolated oocytes was 40 (=2*n*) on average, suggesting that enucleolated oocytes underwent meiosis correctly, and chromosome individualization and condensation at the beginning of the first mitosis (Fig. S1F). However, chromosomes in parthenotes/zygotes from enucleolated oocytes exhibited elongated heterochromatin formation at their proximal ends that are rich in repetitive elements such as telomeres, major and minor satellites, and ribosomal genes (Fig. 1F and Fig. S1G). As a consequence, when chromosomes were segregated at anaphase, formation of lagging chromosomes was observed (Fig. S1H). Moreover, DNA damage in zygotes from enucleolated oocytes was checked using antibodies against histone H2AX phosphorylation at serine 139 (γ-H2AX) (House et al., 2014). A certain number of γ-H2AX foci were observed not only in zygotes from enucleolated oocytes but also in those from control oocytes; however, diffuse γ-H2AX signals that colocalized with CREST diffuse signals, were only observed in zygotes from enucleolated oocytes (Fig. S2). Considering that the defect of chromosome segregation only occurs in parthenotes/zygotes from enucleolated oocytes, we conclude that regions showing diffused signals recognized by both γ-H2AX and CREST are regions crucial for correct chromosome segregation but that the remaining DNA damage regions were not. Collectively, these findings indicate that absence of an oocyte nucleolus causes two mitosis defects – i.e. delay in the first mitosis and abnormal chromosome segregation – that are probably caused by

Journal of Cell Science (2017) 130, 2416-2429 doi:10.1242/jcs.195875

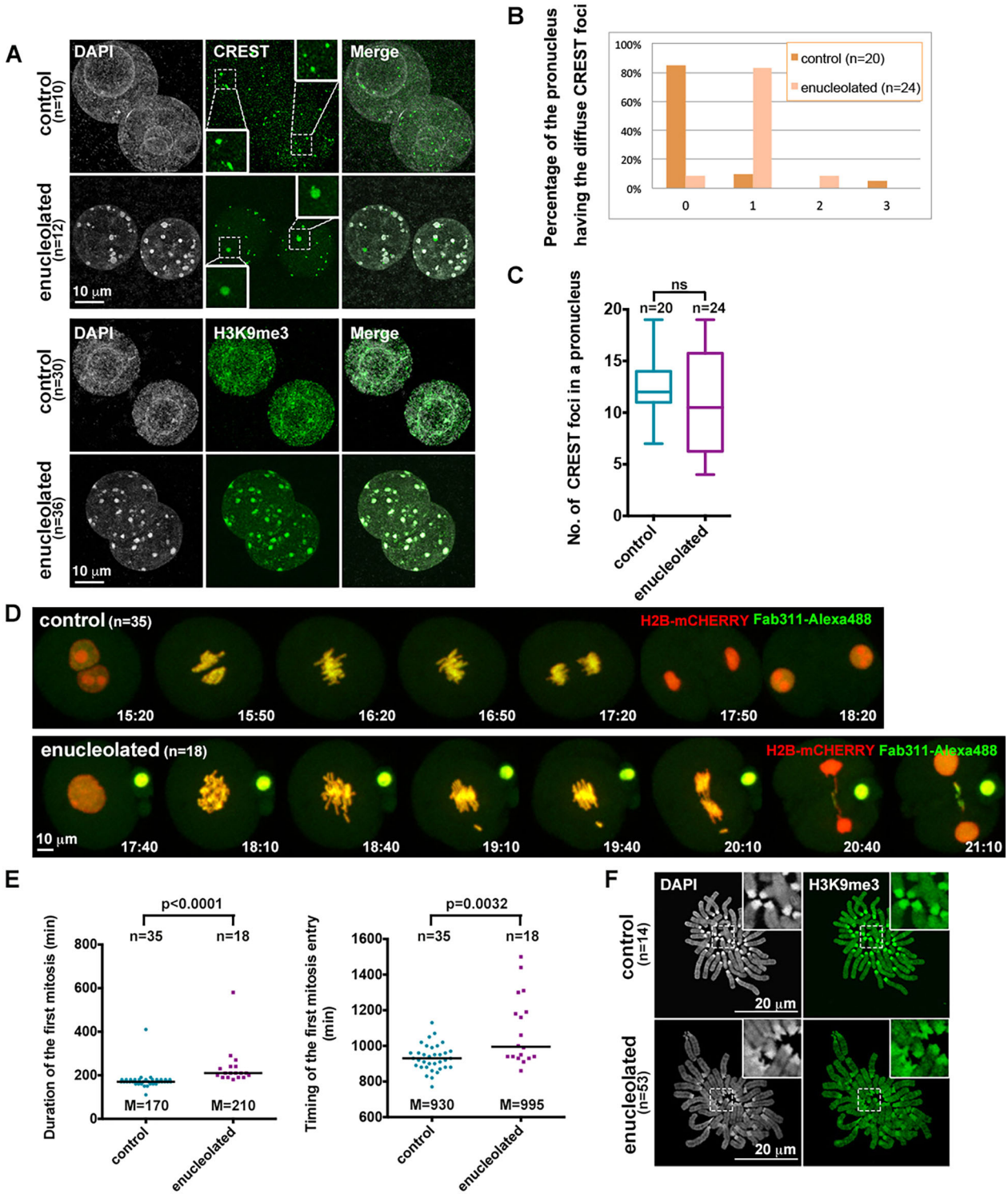

Fig. 1. Loss of the oocyte nucleolus causes disorganization of the higher chromatin in pronuclei and chromosome mis-segregation during the first mitosis in parthenotes from enucleolated oocytes. (A) Immunostaining using parthenotes from enucleolated oocytes 9-12 h after activation with the antibodies a (green). Insets show the diffuse CREST signals (>2 μm^2) in each pronucleus at 2-fold magnification of the regions shown in the dash-lined boxes. DNA was stained with DAPI (gray). Control, parthenotes from nucleolus-reinjected oocytes. (B) Percentage of pronuclei having diffuse CREST signals in parthenotes from control/enucleolated oocytes. The numbers on the *x*-axis of the graph indicate the number of diffuse signals in each pronucleus. (C) Number of CREST foci in each pronucleus of parthenotes from control/enucleolated oocytes. Boxes show the median, 25th and 75th percentiles, and bars show the 10th and 90th percentiles. The number of CREST foci was statistically analyzed by two-tailed Mann–Whitney test. ns, not significant. (D) Representative stills from live cell imaging of parthenotes from control/enucleolated oocytes. Chromosomes were labeled by H2B-mCHERRY (red) and chromosome condensation was visualized by Fab311-Alexa488 (green). Numbers indicate the time after artificial activation (hr:min). (E) The duration and entry timing of the first mitosis in parthenotes are plotted. Bars, median (M). Two-tailed Mann–Whitney test. (F) Representative images of chromosome spreads in parthenotes stained with H3K9me3 antibody (green) and DAPI (gray). Insets show 2.5-fold magnification of the regions shown in the dash-lined boxes. (A-F) n, the numbers of parthenotes measured in three independent experiments.

Journal of Cell Science (2017) 130, 2416-2429 doi:10.1242/jcs.195875

impaired pericentromeric heterochromatin formation. Moreover, as chromosomes in the enucleolated oocytes were segregated correctly during meiosis, removal of a large structure from the nucleus was not a primary cause of the chromosome segregation defects.

The oocyte nucleolus consists of proteins and RNAs

Previous studies reported that some somatic-type nucleolar proteins localize at the oocyte nucleolus only when oocytes were treated with proteinase K or in response to applying an antigen-retrieval protocol (Fulka and Langerova, 2014; Shishova et al., 2015). NPM2 is the only protein whose endogenous localization at the oocyte nucleolus has been observed without any treatment (Inoue and Aoki, 2010). The dearth of reliable information is, at least partly, due to the tight compaction of the oocyte nucleolus, which makes it difficult to detect its components by using immunohistochemistry or other analytical methods (Fig. 2A). To reveal the components of the oocyte nucleolus, isolated nucleoli were digested with the enzymes proteinase K, DNase I and RNase A. The nucleolus treated with proteinase K solution was disassembled within 20 s after treatment. The nucleolus treated with RNase A solution was slightly disassembled after 30 min of treatment, while the nucleolus treated with DNase I solution and that treated with the control solution maintained their structures (Fig. 2B, left). We confirmed the DNase I and RNase A activity by using plasmid DNA and *in vitro*-synthesized RNA as substrates. Both DNase I and RNase A completely digested 0.5 µg substrates soon after treatment, suggesting that both enzymes have high digestion activity, but could not disassemble the oocyte nucleolus efficiently (Fig. 2B, right). Thus, proteins are structurally important for the oocyte nucleolus and, as reported previously, RNAs are also included in the oocyte nucleolus (Shishova et al., 2015).

To identify protein components that are important for the structure of the oocyte nucleolus, we isolated nucleoli from germinal vesicle (GV)-oocytes in two independent sets of experiments (collecting 1200 and 2006 nucleoli each) and determined their protein composition by mass spectrometry (MS) analyses (Fig. 2C,D and Table S2). The proteins found in the control group (ZP1, ZP2, ZP3, ACTB), those involved in the metabolic processes at the cytosol (TKT, LDHB) and HSPA5, which is involved in the unfolded protein response at the endoplasmic reticulum (Hao et al., 2009), were removed from the candidate list. The localization of candidate proteins identified by MS analysis was assessed by the expression of N-terminal eGFP-tagged fusion constructs in GV-oocytes, and NPM2, NCL, SSRP1, and NOLC1 were found to be localized at the nucleolus (Fig. 2E). Because the enucleolation procedure isolates not only nucleoli but also components of the nucleoplasm and cytoplasm from oocytes, the MS analysis also identified nucleoplasmic and cytoplasmic proteins. Moreover, we confirmed that NPM2 was, indeed, located at the oocyte nucleolus by western blotting and immunostaining of cryosections, which revealed NPM2 antigens in the middle of the nucleolus structure (Fig. 2F,G).

Chromosome mis-segregation is also observed in *Npm2*-null parthenotes/zygotes

Next, we analyzed in greater detail the *Npm2*-null oocytes, which lack an apparent nucleolus structure in their GVs and pronuclei (Burns et al., 2003). Chromocenter-like foci were also observed in *Npm2-null* parthenotes/zygotes, and there were one or two diffuse CREST signals in each pronucleus (Fig. 3A,B and Fig. S3A,B). The average number of centromere foci was significantly reduced in the *Npm2*-null parthenotes/zygotes compared with that in heterozygous (het) oocytes (Fig. 3C and Fig. S3C). Thus, centromere proteins were mis-loaded onto the chromatin, and centromere clustering was aborted in *Npm2*-null parthenotes/zygotes.

Live cell imaging of the first mitosis confirmed that *Npm2*-null parthenotes/zygotes underwent the first mitosis cell cycle at the same time as *Npm2*-het parthenotes/zygotes, but showed lagging chromosomes at the first anaphase and formation of abnormal 2-cell embryos with micronuclei (Fig. 3D,E; Fig. S3D,E and Table S1). Thus, the lack of NPM2 caused chromosome mis-segregation during the first mitosis even though the start time of mitosis was appropriate. These results suggest that chromosome lagging during first mitosis is induced by loss of NPM2 in oocytes, and mitosis delay is triggered by the oocyte nucleolus factor triggered by the oocyte nucleolus factor, but not by NPM2. In *Npm2*-null parthenotes/zygotes, the number of chromosomes was 40 (=2*n*), but the elongated heterochromatin formation at the end of chromosomes was also observed in parthenotes/zygotes from *Npm2*-null oocytes, and subsequently the chromosomes were segregated at anaphase, resulting in the formation of lagging chromosomes (Fig. 3F and Fig. S3F-H). Taken together, these results led us to conclude that the nucleolar loss leads to a disorganization of higher-order chromatin structure in pronuclei and frequent chromosome mis-segregation during the first mitosis.

The chromosome segregation defects during the first mitosis, such as chromosome lagging, micronucleus formation and elongated heterochromatin formation at the proximal region of chromosomes at the first mitosis in *Npm2*-null oocytes were similar to those in enucleolated oocytes, and NPM2 was among the most abundant proteins detected, with more than double the number of spectral counts compared to other proteins identified by MS analysis. Thus, we hypothesize that NPM2 is the main and predominant component in the oocyte nucleolus and, therefore, decided to examine whether NPM2 is sufficient to rescue the defects of the enucleolated oocytes.

NPM2 reconstitutes the oocyte nucleolus

We first attempted to identify a set of conditions under which the structure and the function of the nucleolus in *Npm2*-null oocytes is reconstituted by expressing NPM2 again. Thus, we injected *Npm2* mRNA into *Npm2*-null oocytes at second metaphase (MII), and then used these oocytes for IVF and *in vitro* development (IVD). We found that injection of *Npm2* mRNA at a concentration of 1.2 µg/µl, which yielded a much smaller level of NPM2 expression compared to that observed in *Npm2*-het oocytes, resulted in blastocyst formation in only 7% of the injected oocytes (4/54) (Fig. 4A,B). We, therefore, went on to inject 11 µg/µl of *Npm2* mRNA into *Npm2*-null oocytes, resulting in an NPM2 expression comparable to that in *Npm2*-het oocytes (Fig. 4B and Fig. S4A). Expression of NPM2 by injection of *Npm2* mRNA at MII persisted until blastocyst formation (Fig. 4B and Fig. S4B). Then, we fertilized the *Npm2*-null oocytes injected with 11 µg/µl of *Npm2* mRNA and found that they formed nucleoli of apparently normal morphology in their nuclei at zygote and 2-cell stages (Fig. 4C top and D). We noticed small amorphous structures in the nuclei of *Npm2*-null oocytes but their electron-densities and morphological properties were different from those of the oocyte nucleoli (Fig. 4D bottom). Remarkably, we found that the reconstituted nucleoli in the *Npm2*-null zygotes were much larger than those in the controls (Fig. 4C top and D). Considering that the level of NPM2 in the *Npm2*-null oocytes injected with *Npm2* mRNA was higher than that in *Npm2*-het oocytes (Fig. 4B and Fig. S4A), we conclude that

Journal of Cell Science (2017) 130, 2416-2429 doi:10.1242/jcs.195875

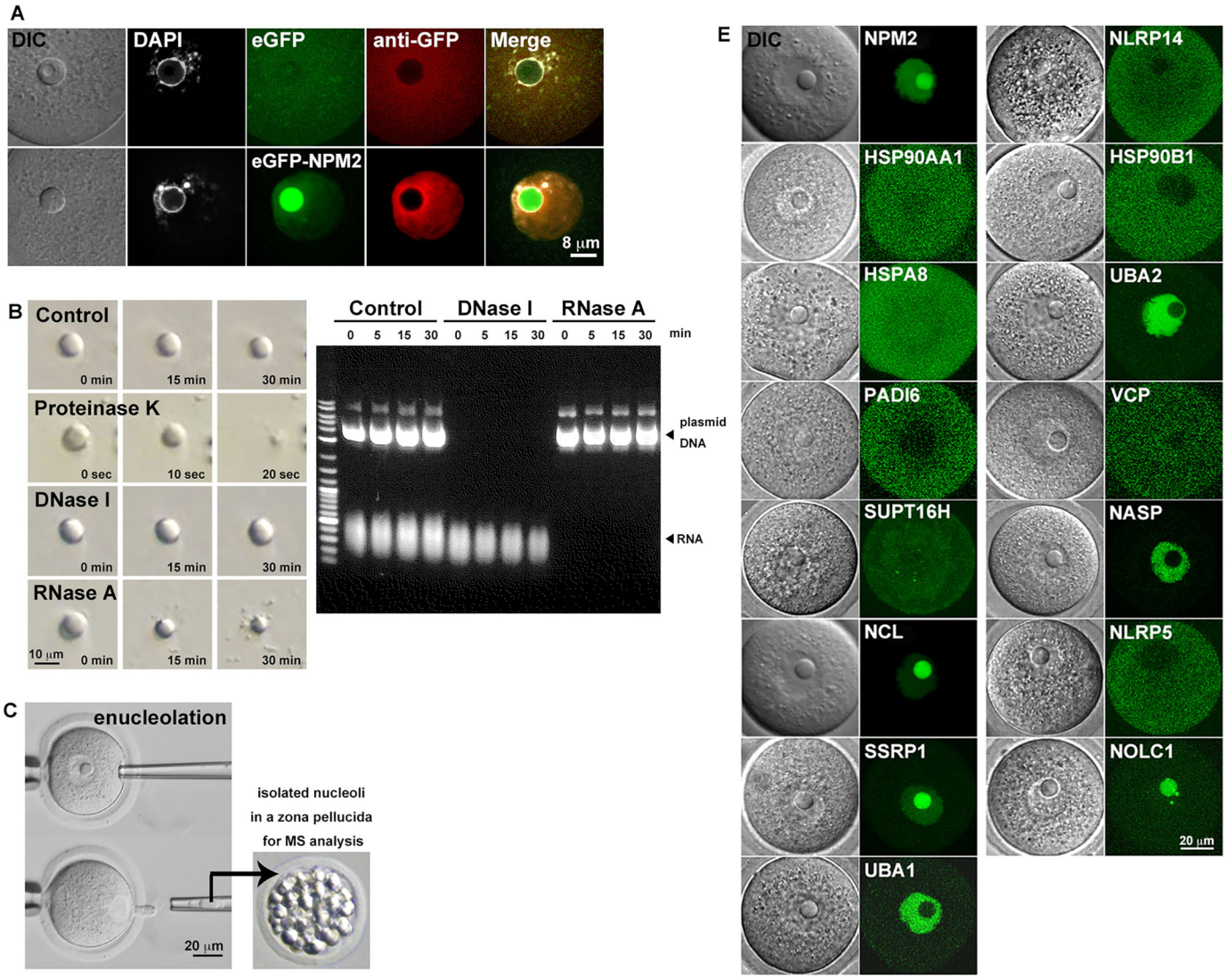

D The top list of proteins identified from nucleoli isolated from mouse GV-oocytes

#	Identified Proteins	Gene Symbol	Accession Number	No of Cleavage	MW (kDa)	Control	Nucleolus
1	Nucleoplasmin-2	Npm2	IPI00330555	31	23	0	89
2	Zona pellucida sperm-binding protein 2	Zp2	IPI00117161	63	80	29	41
3	Heat shock protein HSP 90-alpha	Hsp90aa1	IPI00330804	108	85	0	35
4	Heat shock cognate 71 kDa protein	Hspa8	IPI00323357	81	71	0	33
5	Protein-arginine deiminase type-6	Padi6	IPI00170156	64	77	0	33
6	Zona pellucida sperm-binding protein 3	Zp3	IPI00114128	27	46	26	26
7	FACT complex subunit SPT16	Supt16h	IPI00120344	152	120	0	26
8	Transketolase	Tkt	IPI00137409	65	68	0	25
9	Nucleolin	Ncl	IPI00317794	111	77	0	24
10	L-lactate dehydrogenase B chain	Ldhb	IPI00229510	33	37	0	22
11	Actin, cytoplasmic 1	Actb	IPI00110850	36	42	3	15
12	Isoform 2 of FACT complex subunit SSRP1	Ssrp1	IPI00407571	115	81	0	13
13	Ubiquitin-like modifier-activating enzyme 1	Uba1	IPI00123313	96	118	0	12
14	NACHT, LRR and PYD domains-containing protein 14	Nlrp14	IPI00460862	102	113	0	11
15	Endoplasmin	Hsp90b1	IPI00129526	112	92	0	11
16	SUMO-activating enzyme subunit 2	Uba2	IPI00130173	72	71	0	10
17	phospholipase A2, group IVC isoform 1	Pla2g4c	IPI00465872	77	69	0	9
18	Transitional endoplasmic reticulum ATPase	Vcp	IPI00622235	97	89	0	8
19	Isoform 1 of Nuclear autoantigenic sperm protein	Nasp	IPI00130959	78	84	0	8
20	78 kDa glucose-regulated protein	Hspa5	IPI00319992	86	72	0	8
21	Exportin-2	Cse1l	IPI00112414	87	110	0	7
22	Isoform 3 of NACHT, LRR and PYD domains-containing protein 5	Nlrp5	IPI00128823	122	126	0	7
23	Zona pellucida sperm-binding protein 1	Zp1	IPI00310464	39	69	9	6
24	Nucleolar and coiled-body phosphoprotein 1 isoform D	Nolc1	IPI00719871	118	74	0	6
25	Tubulin alpha-1A chain	Tuba1a	IPI00110753	39	50	0	5

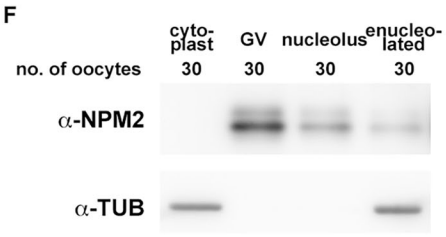

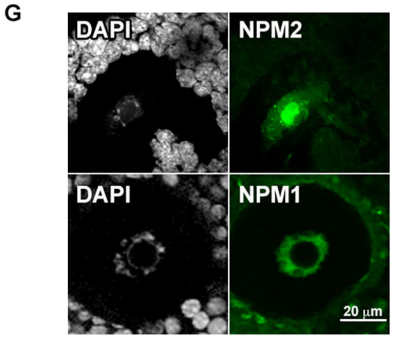

Fig. 2. See next page for legend.

Journal of Cell Science (2017) 130, 2416-2429 doi:10.1242/jcs.195875

Fig. 2. Analysis of the oocyte nucleolus components. (A) The compact structure of the oocyte nucleolus prevents antibody inflow into the structure. EGFP-NPM2 signals (green) in the oocyte nucleolus could not be stained by anti-GFP antibody (red). DNA was stained by DAPI (gray). DIC, differential interference contrast. (B) Components in the oocyte nucleolus were assessed by proteinase K, DNase I, and RNase A (left). The activity of the enzymes was checked at each time point indicated above the gel image. Digestion of DNA and RNA was checked by using 1% agarose gel electrophoresis (right). (C) The method of MS analysis using isolated nucleoli by enucleolation from GV-oocytes. The isolated nucleoli were kept in evacuated zona pellucidae and used for MS analysis. (D) List of identified nucleolus proteins. (E) Localization of MS candidate proteins tagged with eGFP (green) at the N-terminus. DIC, differential interference contrast. (F) NPM2 localization in the oocyte nucleolus was confirmed by western blotting. The oocyte number in each sample is indicated above the blots and α-tubulin (TUB) was used as a loading control (n=3). (G) NPM1 (green) localized at the nucleoplasm and NPM2 localized at the nucleolus in cryosections. DNA was stained by DAPI (gray).

levels of synthesized NPM2 is proportional to the size of the nucleolus. Importantly, 56% (27/48) of the *Npm2*-null oocytes injected with *Npm2*-mRNA at 11 µg/µl reached the blastocyst stage, and 51% (31/61) developed to full term, which is comparable to the rate of blastocyst formation and of development to full-term live births in *Npm2*-null oocytes injected with the isolated nucleoli (Fig. 4A and C bottom; and Table 1). These results indicate that NPM2 expression at MII establishes a situation that rescues the integrity of the nucleolus structure and deals with functional deficiencies of early embryonic development in embryos from *Npm2*-null oocytes.

Next, we investigated whether NPM2 protein expression alone would be sufficient to reconstitute the nucleolus in embryos from enucleolated oocytes. The critical time point at which the oocyte nucleolus is required is the early step of pronucleus formation before the activation of zygotic genes, when zygotes are not able to newly synthesize mRNAs (Aoki et al., 1997; Kyogoku et al., 2014; Ogushi and Saitou, 2010). Therefore, we injected *Npm2*-mRNA (11 µg/µl) into enucleolated oocytes at MII and these oocytes injected showed higher levels of NPM2 protein expression than control oocytes injected with an *eGfp* mRNA (Fig. 5A), were successfully fertilized and, subsequently, formed large nucleoli in their pronuclei of zygotes (Fig. 5B,C). With the expression of NPM2 in zygotes from enucleolated oocytes, the shape of the heterochromatin was restored from a chromocenter-like type to a peri-nucleolar ring type and abnormal diffused CREST signals were not observed (n=28) (Fig. 5C). We also investigated the nascent transcription of total RNA and rRNA by using a bromouridine (BrUTP)-incorporation assay in the absence or presence of the RNA polymerase II inhibitor α-amanitin (Zatsepina et al., 2000). In late 2-cell embryos from enucleolated and *Npm2*-mRNA-injected oocytes, BrUTP incorporation was detected 30 min after BrUTP injection both in the absence and presence of α-amanitin (Fig. S5). Moreover, consistent with a previous report, nascent rRNA transcription was also observed in 2-cell embryos from enucleolated oocytes (Fulka and Langerova, 2014). Therefore, with or without an oocyte nucleolus, the embryos undergo zygotic gene activation and resume rRNA transcription successfully. Strikingly, 48% (33/69) of embryos from enucleolated oocytes injected with *Npm2*-mRNA reached the blastocyst stage (Fig. 6A,B) and 21% (16/78) of the 2-cell embryos from NPM2-rescued enucleolated oocytes developed to full term (Table 1). This demonstrates that NPM2 expression at MII is in itself capable to reconstitute the structural integrity of the nucleolus and to rescue the defects in embryos from enucleolated oocytes.

Formation of the NPM2 pentamer and NPM2 C-terminus are required for the structure and function of the nucleolus

NPM2 consists of an N-terminal core domain followed by a central region comprising two acidic domains (A2, A3) separated by a nuclear localization signal, and also a C-terminal cluster of basic amino acids that is called the the K-rich motif (Fig. 7A). NPM2 has been reported to form homo-pentamers in a manner that depends on the N-terminal core domain (Platonova et al., 2011), whereas the K-rich motif was shown to be required for its localization at the nucleolus (Inoue and Aoki, 2010). To identify the domain of NPM2 that is responsible for oocyte nucleolus formation and rescue of early embryonic development, we constructed two truncation mutants of NPM2, one lacking a K-rich motif (ΔC16) and another lacking a core domain (ΔCore). NPM2 tagged with eGFP at the N-terminus localized predominantly to the nucleolus in oocytes at the GV-stage and in 2-cell embryos but both eGFP-ΔC16 and eGFP-ΔCore concentrated at the nucleoplasm and were excluded from the nucleolus, suggesting that both domains are required for oocyte nucleolus localization and formation (Fig. S6A).

Npm2-wildtype and *Npm2*-het zygotes formed one or several nucleoli in their nuclei 12 h post-fertilization (hpf) and 24 hpf, respectively (Fig. 7B). Consistent with the notion that the protein levels of NPM2 are proportional to the size of the nucleolus, the nucleolus in *Npm2*-het zygotes, which showed a reduced NPM2 level, was smaller than that in *Npm2*-wild zygotes (Fig. 7B,C and Fig. S6B). Neither of the NPM2-truncation mutants rescued the defects in nucleolus formation in zygotes or in early embryonic development of *Npm2*-null oocytes, whereas the full-length NPM2 did (Fig. 7B-D and Table S3). Moreover, when ΔC16 or ΔCore mRNA was injected into *Npm2*-het oocytes, these oocytes, although fertilized, did not form correct chromosomes at the first mitosis and arrested at the 2- to 8-cell stage, suggesting that these truncation mutants dominantly negative affect early embryonic development (Fig. 7D and E). We found that full-length NPM2 and ΔC16 form pentamers both in exogenously expressed HEK293T cells and in the oocytes (Fig. S6C), whereas ΔCore did not. Notably, ΔC16 and ΔCore reduced formation of endogenous NPM2 pentamers, indicating that interruption of endogenous NPM2 pentamer formation by ΔC16 or by ΔCore expression in *Npm2*-het oocytes has dominant-negative effects in chromosome formation and early embryonic development. Alternatively, it is possible that expression of ΔCore, which has a highly acidic region, induced aberrant chromosome decondensation by non-specific binding to basic proteins, such as histones. We conclude that both the N-terminal and the C-terminal domains of NPM2 are essential for the structural integrity and function of the nucleolus.

DISCUSSION

In this report, we show that proteins are necessary for structural integrity of the oocyte nucleolus and demonstrate by proteomics analysis that NPM2, NCL, SSRP1, and NOLC1 contribute to the nucleolus. We also provide evidence that the oocyte nucleolus can be reconstituted structurally and functionally by the expression of NPM2 only. NPM2 belongs to the NPM family of proteins, which consists of NPM1, NPM2 and NPM3. NPM1 and its binding protein NPM3 are nucleolar phosphoproteins and, in somatic cells, are involved in diverse processes, such as ribosome biogenesis and maintenance of genomic stability (Colombo et al., 2011; Okuwaki et al., 2001). NPM2 shares the conserved NPM-core domain at N-terminus with NPM1 and NPM3; however, nucleoplasmin, the NPM2 ortholog in amphibians, has little effect on ribosome biogenesis but is well known as a histone chaperone for sperm

Journal of Cell Science (2017) 130, 2416-2429 doi:10.1242/jcs.195875

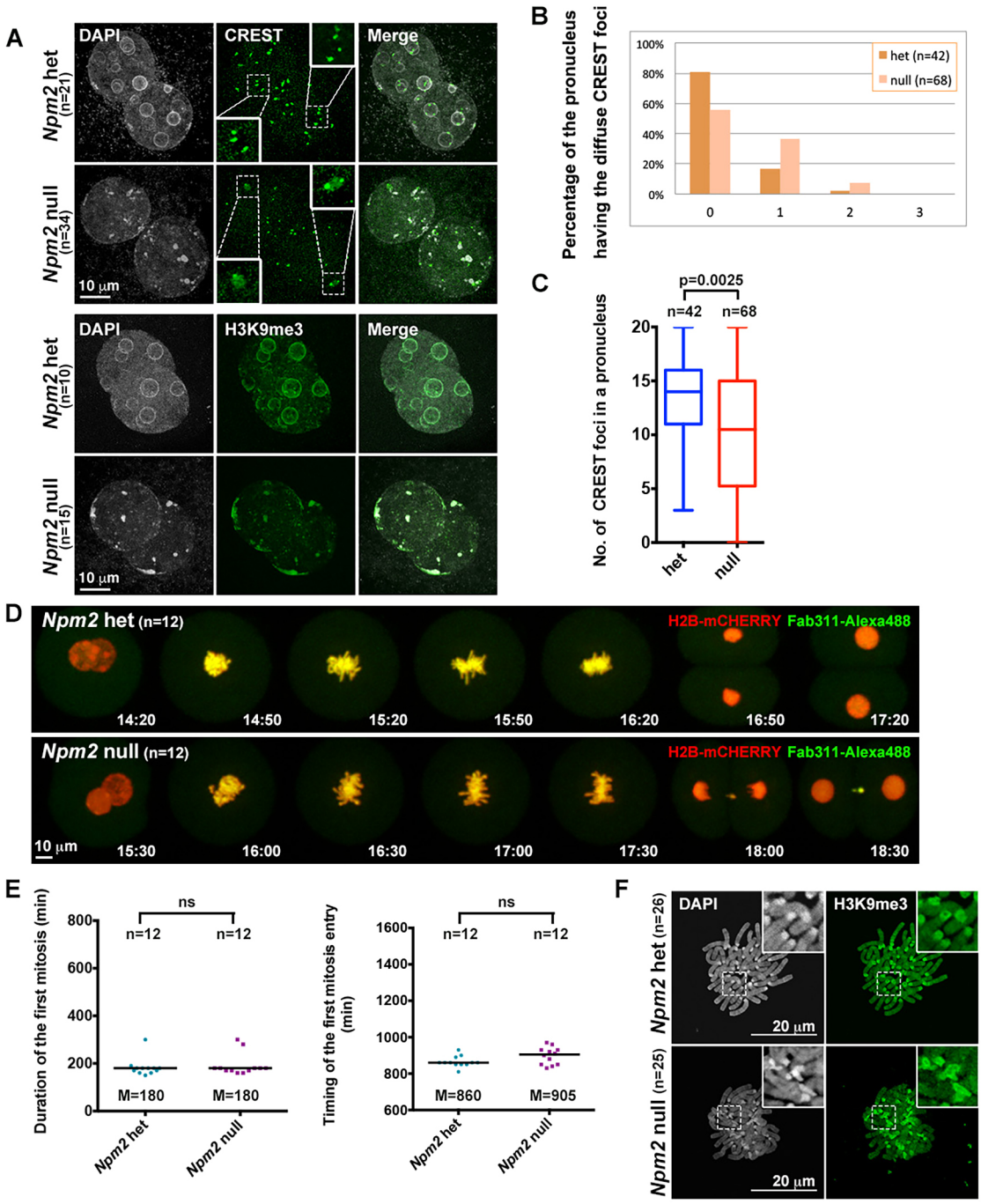

Fig. 3. Parthenotes from *Npm2*-null oocytes show defects similar to those from enucleolated oocytes. (A) Parthenotes from *Npm2*-null oocytes stained with the antibodies as indicated (green) and DAPI (gray). Insets show the diffuse CREST signals at 2-fold magnification. (B) Percentage of pronuclei having diffuse CREST signals in parthenotes from *Npm2*-het/-null oocytes. (C) Number of CREST foci in each pronucleus of parthenotes from *Npm2*-het/-null oocytes. Two-tailed Mann–Whitney test. ns, not significant. (D) Representative stills from live cell imaging of parthenotes from *Npm2*-het/-null oocytes as in Fig. 1C. (E) The duration and entry timing of the first mitosis in parthenotes are plotted. Bars, median (M). Two-tailed Mann–Whitney test. (F) Representative images of chromosome spreads in parthenotes stained with H3K9me3 antibody (green) and DAPI (gray). Insets show 2.5-fold magnification of the regions shown in the dash-lined boxes. (A-F) n, the numbers of parthenotes measured in three independent experiments.

chromatin decondensation (Laskey et al., 1978; Philpott et al., 1991). In our study, both parthenotes and zygotes from enucleolated and *Npm2*-null oocytes showed defects in centromere clustering and in centromeric/pericentromeric chromatin organization in their pronuclei. Therefore, in contrast to *Xenopus* nucleoplasmin, which is required for paternal chromatin remodeling, mouse NPM2 is required for both paternal and maternal chromatin remodeling, especially at the centromeric/pericentromeric regions. Because of the complexity of biochemical experiments when using mammalian oocytes, there are few biochemical data of mammalian NPM2 to specify its molecular function. However, one can speculate about the function of NPM2 by comparing it to NPM1 in somatic cells and to nucleoplasmin-like protein (NPL) in *Drosophila*, since both proteins have the conserved region of the

Journal of Cell Science (2017) 130, 2416-2429 doi:10.1242/jcs.195875

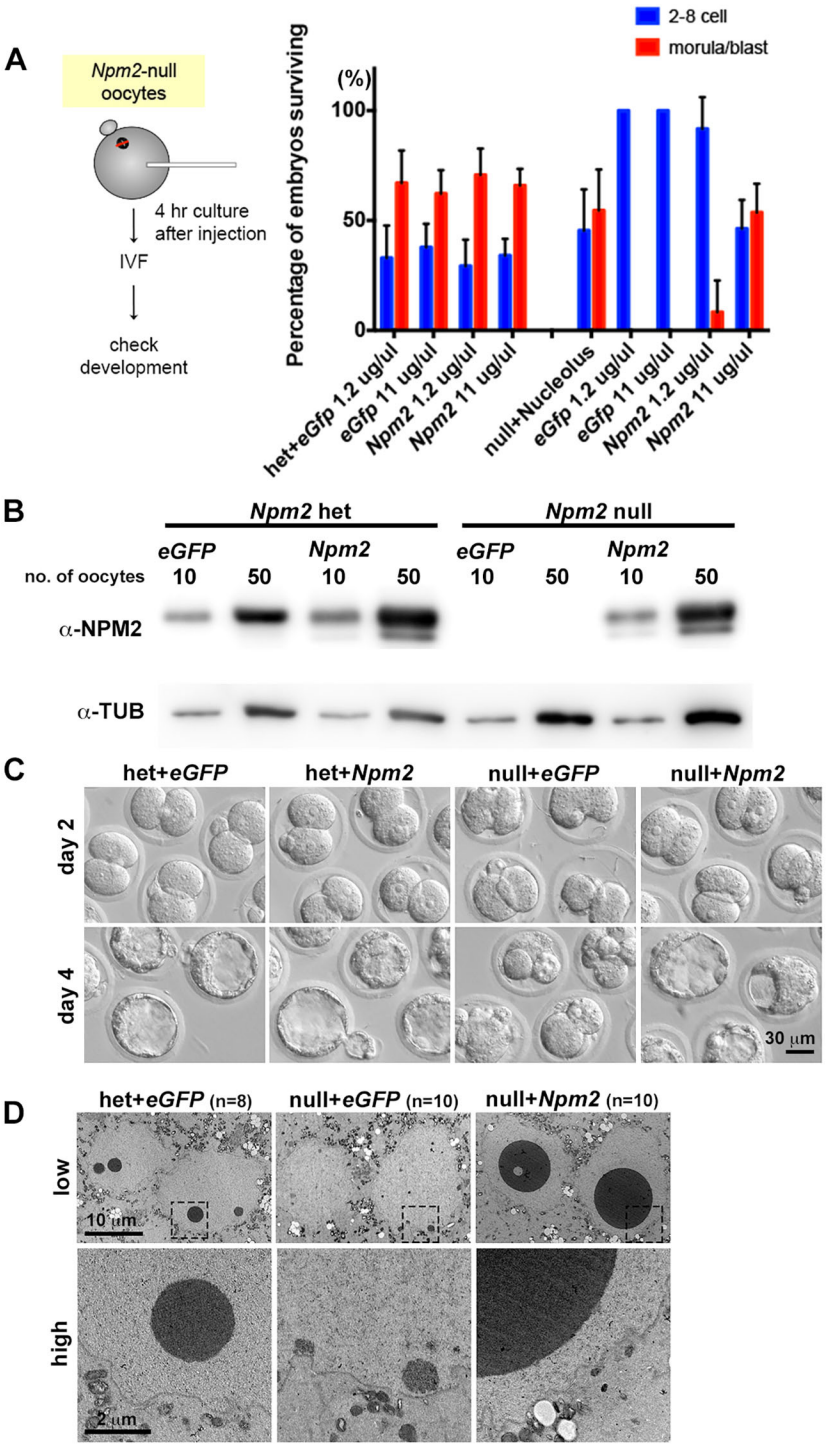

Fig. 4. NPM2 expression in oocytes at second metaphase rescues the defects of *Npm2*-null embryos in early embryonic development. (A) Schematic of the rescue experiments in *Npm2*-null oocytes. IVF, *in vitro* fertilization. The graph shows the percentage of mRNA-injected embryos that reached the blastocyst stage. Error bars, +s.d. (*n*>3 each). (B) NPM2 protein expression levels in *Npm2*-het/-null oocytes injected with the indicated mRNAs at the concentration of 11 µg/µl. The oocyte number in each sample is indicated above the blots; α-tubulin (TUB) was used as a loading control (*n*=3). (C) Representative images of embryos from *Npm2*-het/-null oocytes rescued by the indicated mRNAs at 2 and 4 days after IVF. (D) Transmission electron microscopy (TEM) images of pronuclei in zygotes from *Npm2*-het/-null oocytes rescued by *Npm2*-mRNA injection. Bottom panels show 5-fold magnifications of the regions in the dash-lined boxes. n, number of zygotes measured in three independent experiments.

NPM-core domain and also form a spherical body (Liu et al., 2006; Mitrea et al., 2016). For example, NPM1, has the ability to bind to the centromere-specific nucleosome CENP-A and is required for proper kinetochore and microtubule attachments (Amin et al., 2008; Dunleavy et al., 2009; Foltz et al., 2009). Moreover, the deletion of NLP in S2 cells showed similar defects to those in parthenotes/zygotes from enucleolated and *Npm2*-null oocytes (Liu et al., 2006; Padeken et al., 2013), and NLP binds to CTCF and the centromere-specific nucleosome CenH3, as well as to the NCL homolog Modulo, whose binding is required for centromere clustering to the nucleolus. Since NCL is one of the oocyte nucleolus proteins that was identified in our proteomics analysis as well as in other studies (Fulka and Langerova, 2014; Shishova et al., 2015), it is highly possible that NPM2 binds to NCL and is involved in centromere clustering to the nucleolus and regulation of the centromeric/pericentromeric chromatin organization in interphase, which is required for correct chromosome segregation.

Our study, pericentromeric heterochromatin in the pronuclei of parthenotes/zygotes from enucleolated and *Npm2*-null oocytes showed atypical diffuse CREST signals and chromocenter-like structures that are never observed in embryos before the embryonic

Journal of Cell Science (2017) 130, 2416-2429 doi:10.1242/jcs.195875

Table 1. Developmental potency of embryos from *Npm2*-het/-null and control/enucleolated oocytes injected with *Npm2* mRNAs

		eGfp	*Npm2*	*Npm2*
Oocytes	Nucleolus	11 µg/µl	1.2 µg/µl	11 µg/µl
Npm2 het	24/40	19/40	18/40	22/40
Npm2 null	18/40	0/60	0/62	31/61
Control	–	9/60	10/60	12/60
Enucleolated	–	0/60	0/62	16/78

Numbers show the total of pups obtained per total of transferred embryos.

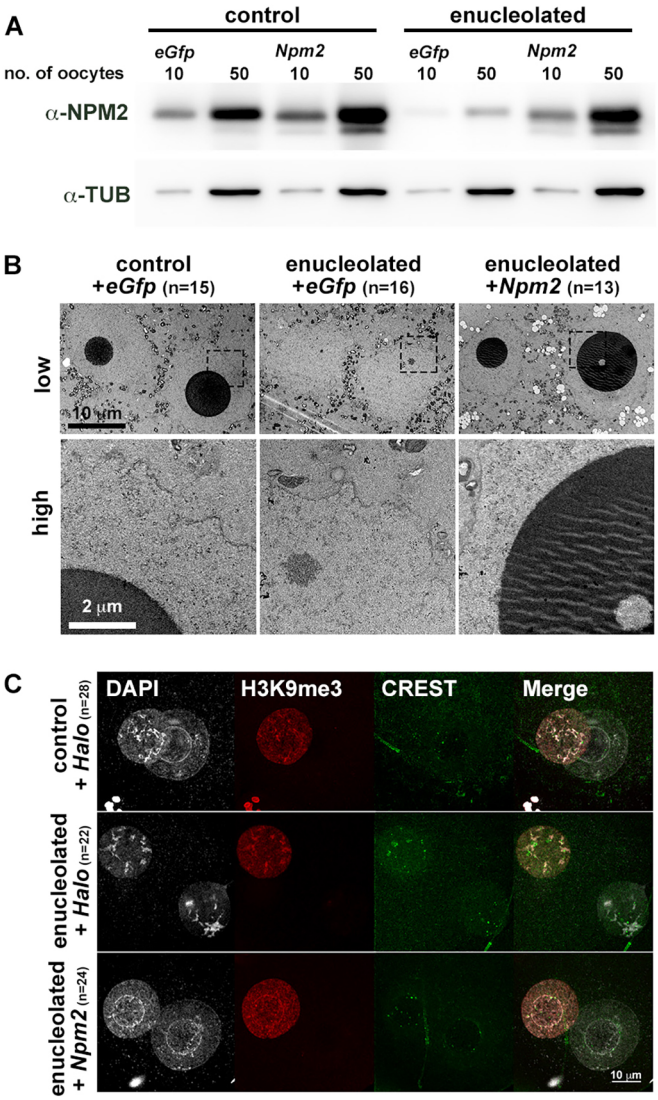

Fig. 5. Expression of NPM2 alone is sufficient to reconstitute the nucleolus structure of pronuclei in zygotes. (A) NPM2 protein expression levels in control/enucleolated oocytes injected with the indicated mRNA. The oocyte number in each sample is indicated above the blots and α-tubulin (TUB) was used as a loading control (*n*=3). Control, zygotes from nucleolus-reinjected oocytes. (B) Transmission electron microscopy (TEM) images of pronuclei in zygotes from control/enucleolated oocytes rescued by *Npm2*-mRNA injection. Bottom panels show 5-fold magnifications of the regions in the dash-lined boxes. (C) Immunostaining using zygotes from NPM2-expressing enucleolated oocytes 9-12 h after fertilization with antibodies as indicated. For injection control at MII oocytes, *Halo* mRNA at 10 µg/µl was injected into control and enucleolated oocytes as *Npm2* mRNA. (B,C) n, number of zygotes measured in three independent experiments.

genome activation. It is known that the expression of major satellite repeats induces the reorganization of pericentromeric heterochromatin from peri-nucleolar rings into chromocenters (Probst et al., 2010). However, Fulka and Langerova (2014), have reported the transcriptional repression of major satellites in zygotes from enucleolated oocytes, which is inconsistent with the phenotype of ectopic formation of chromocenters. Therefore, the question whether the nucleolus/NPM2 is involved in the reorganization of pericentromeric heterochromatin via transcriptional regulation of major satellite repeats remains to be answered. Moreover, if so, how do the nucleolus or NPM2 control this process.

Consistent with previous reports, we found that the embryos without oocyte nucleolus components have the ability to resume transcription of rRNA and to synthesize proteins in the same manner as control embryos do, suggesting that the oocyte nucleolus has little effect on ribosome biogenesis (Fulka and Langerova, 2014; Kyogoku et al., 2014; Ogushi et al., 2008). This naturally raises the question, what is the function of the oocyte nucleolus? Our study did not provide a clear answer but recent reports by the groups of Brangwynn, Hyman, and Rosen have provided some suggestions. Based on their observations, these groups claimed that non-membranous organelles that consist of nucleic acids and proteins form liquid-like droplets through phase separation from surrounding environments, a phenomenon that is important for the spatiotemporal control of proteins while maintaining their dynamics with the surrounding organelles or nucleo-cytoplasm (Banani et al., 2017; Bergeron-Sandoval et al., 2016; Brangwynne, 2013; Shin et al., 2017). In somatic cells, NPM1 – one of the NPM2 homologs – undergoes phase separation in a concentration-dependent manner together with the arginine-rich proteins and rRNAs that are required for ribosome biogenesis. This event is critical for structural organization of the somatic nucleoli and, presumably, required to control the activity of ribosome biogenesis (Feric et al., 2016; Holmberg Olausson et al., 2014; Mitrea et al., 2016). In our study, we found that NPM2 has the ability to form a spherical body together with other proteins and RNAs in a concentration-dependent manner. However, it remains to be elucidated whether this NPM2 body has biophysical and functional properties that are similar to those of the liquid-like body, and whether NPM2-body formation during oogenesis occurs due to an enhancement of reactions among components of the oocyte nucleolus or because NPM2 and binding components from surrounding environments are excluded in order to prevent non-favorable reactions in the interphase nucleus.

The molecular function of NPM2 is still unclear but we have clarified here the timing of the NPM2 requirement during oogenesis and early embryogenesis. NPM2 is expressed in all stages of oocytes – from primordial follicles to antral follicles and in those of embryos from zygotes to morulae (Burns et al., 2003; Inoue and Aoki, 2010), but NPM2 protein expression in oocytes at MII rescued the defects in early embryonic development in *Npm2*-null oocytes. Thus, NPM2 does not have any roles in oocyte growth but is required for the processes after fertilization. Considering that the oocyte nucleous is required at the timing of the early step of pronucleus formation and the nucleolus can be reconstitued by NPM2 protein expression, it appears that NPM2 is required during this step, i.e. when chromatin remodeling and nuclear body reassembly occur (Kyogoku et al., 2014; Ogushi and Saitou, 2010).

We have demonstrated here that the oocyte nucleolus structure can be reconstituted by expressing a single protein – NPM2 – and that an NPM2-based nucleolus structure serves as a key platform to organize pericentromeric heterochromatin in order to correctly segregate parental chromosomes.

Journal of Cell Science (2017) 130, 2416-2429 doi:10.1242/jcs.195875

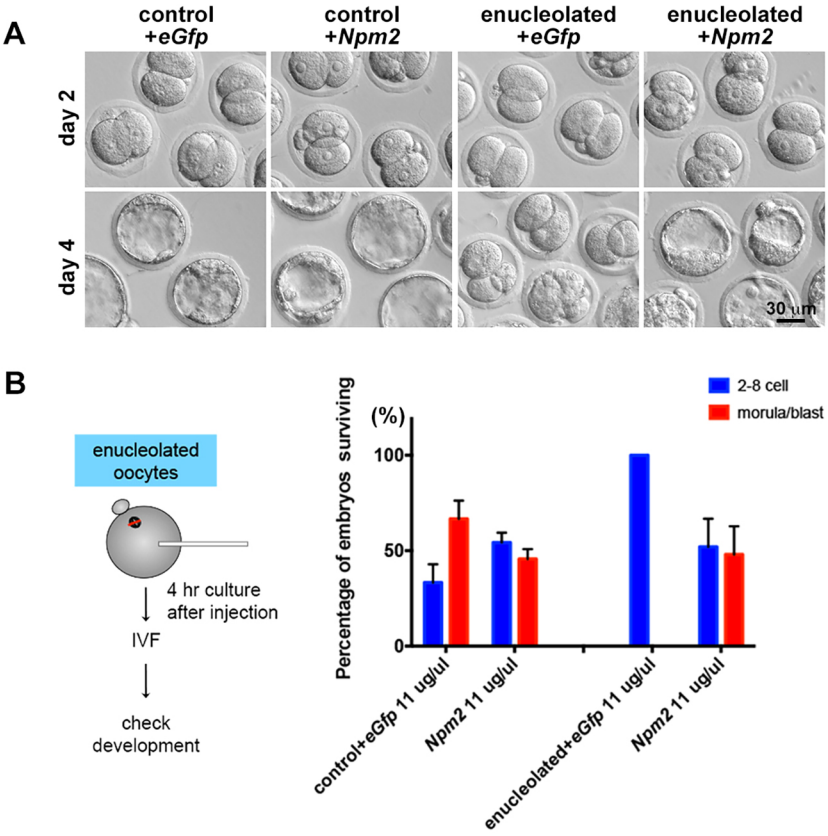

Fig. 6. NPM2 expression rescues the defect caused by loss of the oocyte nucleolus in early embryonic development. (A) Representative images of embryos from control/enucleolated oocytes rescued by the indicated mRNAs at 2 and 4 days after IVF. (B) Schematic of the rescue experiments in enucleolated oocytes. IVF, *in vitro* fertilization. The graph shows the percentage of mRNA-injected embryos that reached the blastocyst stage. Error bars, +s.d. (n>3 each).

MATERIALS AND METHODS

Animal maintenance, handling and care, and mouse strains

All animals were treated with appropriate care according to the ethics guidelines of RIKEN, Kyoto University (Japan) and the University of Oxford (UK). *Npm2* heterozygous (*Npm2*-het) and null (*Npm2*-null) mice were obtained by crossing *Npm2*-het females and *Npm2*-null males (Burns et al., 2003).

Enucleolation and enucleation

Oocytes at the germinal vesicle (GV)-stage were collected from ovaries of B6DBA2F1 females at 8–12 weeks of age at 44–48 h after injection with 7.5 IU equine chronic gonadotropin (eCG; ASKA Pharmaceutical). Fully grown GV-oocytes were released from ovarian follicles by puncture with needles in modified human tubal fluid (HTF) medium (Nippon Medical & Chemical Instruments) supplemented with 200 µM N6, 2′-*O*-dibutyryladenosine 3′,5′-cAMP sodium salt (dbcAMP; Sigma) and 100 µM 3-isobutyl-1-methylxanthine (IBMX; Sigma), and their cumulus cells were removed by gentle pipetting. For the *in vitro* maturation (IVM) medium, minimum essential medium (MEM; Sigma) containing 10% fetal bovine serum (FBS; Equitech Bio), 250 µg/ml sodium pyruvate and 8 µg/ml kanamycin was used. GV-oocytes were cultured for 3-4 h in IVM medium containing 200 µM dbcAMP and 100 µM IBMX at 37°C under an atmosphere of 5% CO_2, and then manipulated with a micromanipulator equipped with a PIEZO drive (Prime Tech). Enucleolation (Fulka Jr et al., 2003; Ogushi et al., 2008) and enucleation (Fulka and Fulka, 2007) were performed in modified HTF medium with 200 µM dbcAMP, 100 µM IBMX and 10-15 µg/ml cytochalasin D (Sigma) under an inverted microscope (Olympus IX71) equipped with a micromanipulator (Narishige). Enucleolated oocytes that had been reinjected with a nucleolus served as a control. After 1 h of recovery culture in IVM medium with dbcAMP and IBMX, the control and enucleolated oocytes were washed and cultured with IVM medium to resume meiosis. Nucleoli isolation was performed by enucleolation, and isolation of GVs and cytoplasts was done by enucleation; these samples were used for enzyme digestion, MS analysis or immune-blot analysis.

In vitro fertilization, parthenogenetic activation and intracytoplasmic injection

For *in vitro* fertilization (IVF), spermatozoa were obtained from the caudal epididymides of ICR males at 10-14 weeks of age and cultured for 2 h in HTF medium (Quinn et al., 1985) to induce capacitation. After 18-20 h of IVM, control and enucleolated oocytes at second metaphase (MII) were inseminated with capacitated spermatozoa at a concentration of 2.0×10^7 sperm/ml for 4-6 h in HTF medium. In *Npm2*-het/-null mice, oocytes at MII were collected from oviducts of 8–12-week-old females that had been injected with 7.5 IU of eCG followed 48 h later by 7.5 IU of human chorionic gonadotropin (hCG; ASKA Pharmaceutical), and inseminated with spermatozoa at the concentration of 2.0×10^6 sperm/ml for 4-6 h in HTF medium. For parthenogenetic activation, oocytes at MII were artificially activated by treating them with modified Tris-buffered medium (20 mM Tris, 113 mM NaCl, 3 mM KCl, 11 mM glucose, 5 mM Na pyruvate, and 2 mg/ml BSA) or Ca^{2+}-excluding CZB medium (Chatot et al., 1989) containing 5–10 mM $SrCl_2$ and 5 µg/ml cytochalasin B for 4 h. For intracytoplasmic injection (ICSI), epididymal spermatozoa were capacitated in CZB medium for 1 h, and resuspended in HEPES-CZB medium containing 12% polyvinylpyrrolidone (Wako Chemicals). Oocytes at MII were placed in HEPES-CZB, and a sperm head isolated by several PIEZO pulses was injected into oocytes under an inverted microscope equipped with a micromanipulator. These oocytes were then transferred to K^+- supplemented simplex optimised medium (KSOM; Millipore) or CZB medium in order to assess the progression of early-embryonic development.

Whole-mount immunofluorescence

Cultured oocytes and parthenotes/zygotes were fixed in 2% paraformaldehyde (PFA) in PBS or in 20 mM Tris-HCl, pH 7.5, and 150 mM NaCl (KB) for 30 min. After permeabilization with 0.2% Triton X-100 in PBS or in KB overnight at 4°C, oocytes and parthenotes/zygotes were incubated for 1 h in PBS or KB with 5 mg/ml BSA at room temperature, and incubated with primary antibodies overnight at 4°C. Following three washes with PBS or KB, Alexa-Fluor-labeled secondary

Journal of Cell Science (2017) 130, 2416-2429 doi:10.1242/jcs.195875

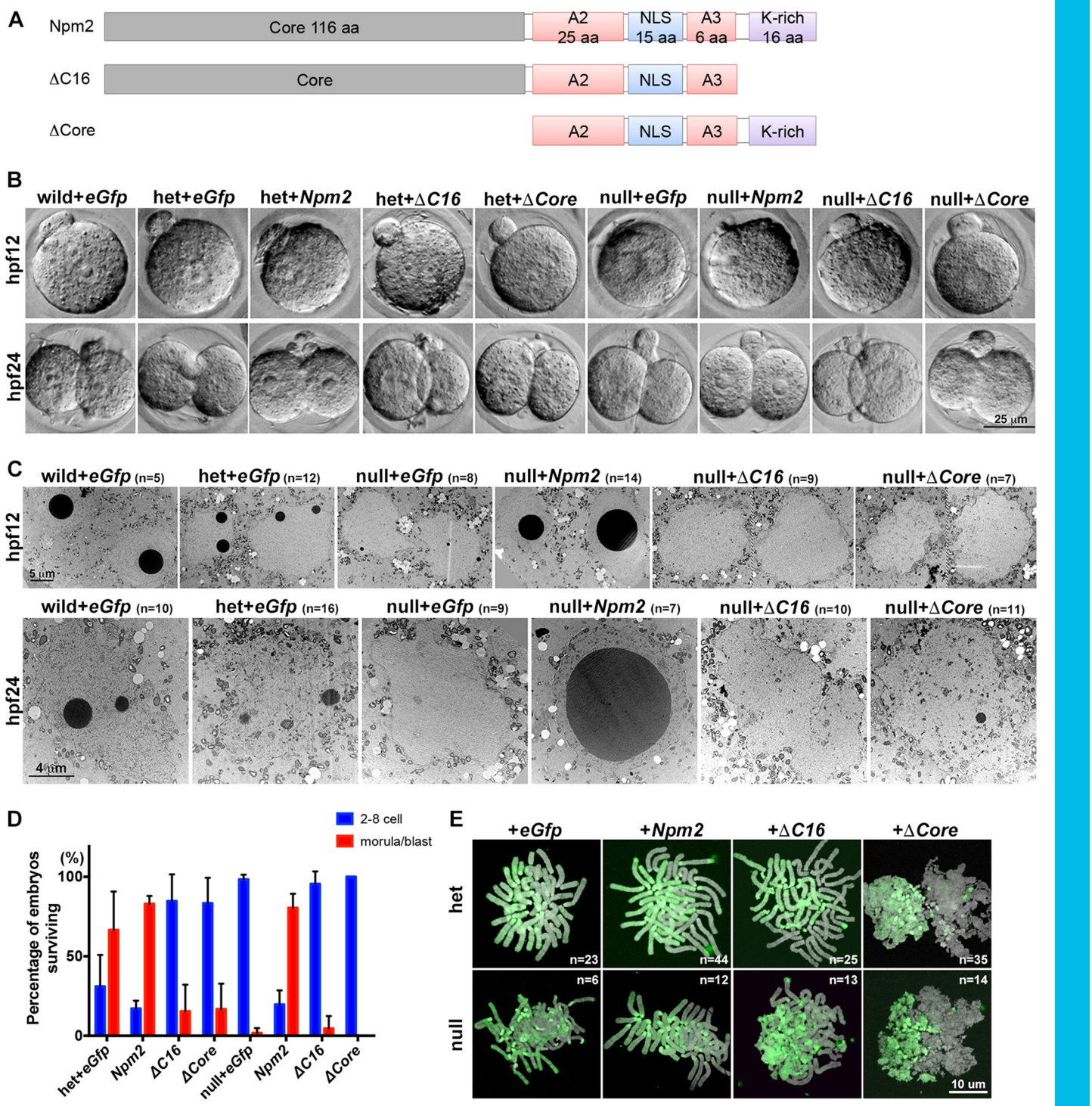

Fig. 7. Both the N-terminal and the C-terminal domains are essential for the structural integrity and function of NPM2. (A) Schematic of NPM2-truncation mutants. NPM2 has a core domain, two acidic domains (A2 and A3), a nuclear localization signal (NLS) and a basic cluster, the K-rich motif. (B) Nucleolus formation in embryos at 12 h or 24 h post-fertilization (hpf) from *Npm2*-wild/-het/-null oocytes injected with the indicated mRNAs. (C) Representative TEM images in embryos from *Npm2*-wild/-het/-null oocytes injected with the indicated mRNAs. (D) Percentage of embryos from *Npm2*-het/-null oocytes injected with *Npm2*-truncated mutant mRNAs that reached the blastocyst stage. Bars, SD (n>3 each). (E) Representative images of chromosome spreads in zygotes from *Npm2*-het/-null oocytes injected with *Npm2*-truncated mutant mRNA. Chromosomes were stained with H3K9me3 antibody (green) and DAPI (gray). (C,E) n, the numbers of zygotes/embryos measured in three independent experiments.

antibodies (Invitrogen) were used for the detection of signals and DNA was counterstained with 14.3 μM 4′,6-diamidino-2-phenylindole, dihydrochloride (DAPI). The following primary antibodies were used: anti-HISTONE H3 (trimethyl K9) (Abcam #ab8898, 1:250-400), CREST serum (a kind gift from Y. Muro, Nagoya University, Japan; 1:2000), anti-GFP (Nacalai Tesque, GF090R, #04404-84, 1:200), anti-Phospho-HISTONE H2AX (S139) (γ–H2AX, Cell Signaling #2577, 1:200) and anti-NPM2 (Burns et al., 2003; 1:200–1:400). The samples were mounted with Vectashield mounting medium (Vector Laboratories) and observed under an Olympus FV-1000 confocal microscope or a Zeiss LSM780 confocal

microscope. For detection and analysis of pronuclei in parthenotes/zygotes, samples were scanned in three dimensions and sectioned into *z*-series of 0.3−1.0 µm slices; then the slices were combined and maximally projected by Image J. The area of centromere foci in pronuclei was determined by using the threshold function and were calculated by using Image J. The foci with an area of 0.2−2.0 µm^2 were defined as normal and those with an area of >2.0 µm^2 were defined as diffuse.

Chromosome spread

The zona pellucida of parthenotes or zygotes at the first mitosis was removed by treatment with acidic Tyrode's solution (Sigma); then, the parthenotes/zygotes were placed on a glass slide that had been dipped in a solution of 1% PFA in destilled water, pH 9.2, containing 0.15% Triton X-100 and 3 mM dithiothreitol. Following overnight fixation in a humid chamber, the slide was washed in 0.4% Photoflo (Kodak) in destilled water and dried for 30 min at room temperature. The samples were washed in PBS and then incubated with anti-HISTONE H3 (trimethyl K9) antibody (1:250−1:400) overnight at 4°C. After washing with PBS, the samples were incubated with Alexa-Fluor-488-conjugated donkey anti-rabbit IgG for 1.5 h at room temperature and mounted with Vectashield containing DAPI (Vector Laboratories).

Live cell imaging

To visualize the chromatin and chromosome condensation status, oocytes at MII were injected with *H2b-mCherry* mRNA at 200 ng/µl, and Fab311 antibody conjugated to Alexa-Fluor-488 (Fab311-Alexa488) at 1 µg/µl, which recognizes the phosphorylated Ser10 of histone H3. After injection, oocytes were cultured for 2−4 h in IVM medium to express mRNAs. Following artificial activation or ICSI, oocytes were transferred to 4 µl drops of CZB medium on a glass-bottomed dish and placed in an incubator (MI-IBC; Tokai Hit) at 37°C under 5% CO_2 in air. Observation was performed under an inverted microscope (IX-71; Olympus) equipped with a Nipkow disk confocal unit (CSU-10; Yokogawa Electric Corp.). This system was housed in a dark room at 30°C. Device control and image analysis were performed using MetaMorph software (Molecular Devices). For time-lapse observations, images were taken at 10 min intervals. At each time point, 51 fluorescent images were taken 2 µm apart at the *z*-axis for optical sectioning.

Treatment with proteinase K, DNase I and RNase A

To determine the components of the oocyte nucleoli, isolated nucleoli were treated with proteinase K (Roche) at 2 µg/10 µl, Turbo DNase I (Ambion) 1 U/ 10 µl and RNase A at 0.25 U/10 µl in modified HTF medium without BSA, and were observed under an inverted microscope (Olympus IX71). To check the activity of DNase I and RNase A, 0.5 µg circular plasmid DNA, pCS2-*DsRed* and 0.5 µg *in-vitro* synthesized RNA, *DsRed-Pias I* in 10 µl of modified HTF medium without BSA were treated with each enzyme as described above and kept in liquid nitrogen. After digestion, samples were treated with proteinase K at 200 µg/ml for 10 min at 50°C and enzymes were inactivated by boiling for 5 min at 95°C. DNA and RNA were separated by electrophorese using 1% agarose gel.

Mass spectrometry analysis

The nucleoli isolated from GV-oocytes by enucleolation were kept in evacuated zona pellucidae and used for mass spectrometry (MS) analysis (*n*=2; the numbers of nucleoli and those of zona pellucidae were 1200 or 2006 and 20 or 33, respectively). Nucleolar proteins were loaded on a NuPAGE™ 4−12% Bis−Tris gel and separated in 3-(*N*-morpholino) propanesulfonic acid (MOPS) buffer until SERVA Blue G reached the middle of the gel; then gel was stained with Coomassie G-250 (Invitrogen) and those areas of the gel containing proteins was cut into nine sections. After in-gel digestion with modified trypsin, the resulting peptides were analyzed by liquid chromatography (LC)-MS by using an LXQ linear ion trap mass spectrometer equipped with a nano-ESI source (Thermo Finnigan). From one sample, analysis of LC-MS was performed twice for technical duplication. The ion spectrum data were screened against the NCBI non-redundant protein database with the Mascot program (Matrix Science) and the International Protein Index database (mouse IPI http://www.ebi.ac.uk/IPI/IPImouse.html) was used to identify the proteins (Nozawa et al., 2010).

Plasmid construction and mRNA preparation

All protein cDNA identified by MS analysis was amplified from mouse ovary cDNAs by PCR, then subcloned into pCS2 or pCS2-*eGfp* (a kind gift from J. Lee, Kobe University, Japan). *Npm2*-truncated mutants were kindly provided by F. Aoki (Tokyo University, Japan) and subcloned into pCS2 or pCS2-*eGfp*. pcDNA3-*H2b-mCherry* was generously provided by T. Abe and T. Fujimori (RIKEN CDB, Japan). pHTN was purchased from Promega (#G7721). After confirmation of the sequence in each plasmid, 5 µg of plasmids were linearized by an appropriate restriction enzyme shortly after the sequence of the poly-A signal and transcribed *in vitro* for 2−4 h at 37°C by using an mMESSAGEmMACHINE kit containing the appropriate RNA polymerase (Ambion). Following Turbo DNase I digestion for 15 min at 37°C, RNA was precipitated by lithium chloride, and resuspended in nuclease-free H_2O. Each RNA was aliquoted and stored at −80°C until use.

Localization of eGFP signals in oocytes at the GV-stage and in parthenotes/embryos

Oocytes at the GV-stage that had been cultured for 2−3 h in IVM medium with dbcAMP and IBMX, were injected with mRNAs at 500 ng/µl. They were then further cultured for 4−6 h to induce mRNA expression. In the case of embryos, oocytes at MII were injected with mRNAs at 50−1000 ng/µl, cultured an additional 4 h for mRNA expression and then activated and/or fertilized. eGFP signals were observed under an inverted microscope (Olympus IX71) during epi-fluorescence illumination provided by a Xenon lamp.

Cryosection preparation

Ovaries were collected from ICR females at 3−4 weeks and washed three times in PBS containing 0.2% Tween20 (PBST) for 10 min at 4°C. Ovaries were soaked in a sucrose in PBS gradient of 10−30%, then embedded in optimal cutting temperature (OCT) compound (Sakura Finetek), frozen and sectioned at a thickness of 8−9 µm at −20°C. Air-dried sections were washed three times in PBS and fixed with 2% PFA in PBS for 30 min. After three washes in PBS containing 0.01% polyvinyl alcohol (PBS-PVA), samples were permeabilized in 0.1% Triton X-100 in PBS-PVA, incubated in the blocking solution (3% BSA, 0.1% Tween20, PBS-PVA) and then incubated with antibodies against NPM2 (1:200) or NPM1 (Sigma, FC82291, #B0556, 1:200) in staining solution (1% BSA, 0.1% Tween20, PBS-PVA) overnight at 4°C. After washing with PBS-PVA three times, samples were incubated in staining solution containing secondary antibodies. Samples were then washed three times with PBS-PVA and mounted with Vectashield containing DAPI.

Nucleolus reconstitution

For nucleolus reconstitution experiments, *Npm2* mRNA, *eGfp* mRNA, *Halo* mRNA or the nucleolus from GV-oocytes was injected into control/enucleolated or *Npm2*-het/-null oocytes at MII with the assistance of a PIEZO impact drive unit that allowed the use of an injection pipette with a slightly wider bore. After 4 h of culture in IVM medium, the injected oocytes were subjected to IVF and IVD as described above.

Embryo transfer

Two-cell embryos arising from *Npm2* mRNA or nucleolus-injected oocytes were transferred into the oviducts of d-0.5 pseudo-pregnant ICR female mice at 8−12 weeks of age. Caesarian section was performed at E19.5 and surviving pups were fostered by ICR foster mother that had given birth the previous or the same day.

BrUTP-incorporation assay

In general, we followed the procedure developed by Zatsepina et al. (2000). Briefly, to detect nascent transcripts of total RNA or rRNA, 1 pl of 100 mM 5-bromourudine 5′-triphosphate (BrUTP) in an injection buffer (140 mM KCl, 2 mM PIPES pH 7.4) with or without 50 µg/ml α-amanitin was injected into one blastomere of 2-cell parthenotes 38-40 h after artificial

activation. Another blastomere was used as a negative control of BrUTP incorporation. Only for the detection of rRNA nascent transcripts, 2-cell parthenotes were cultured for 30 min in KSOM containing 10 µg/ml α-amanitin prior to injection of BrUTP. 30-45 min after injection, parthenotes were fixed in 3% PFA in PBS-PVA for 30 min and permeabilized in 0.5% Triton X -100in PBS for 10 min. They were then incubated for 1 h in PBS with 5 mg/ml BSA at room temperature, and reacted with a primary antibody, anti-Bromodeoxyuridine (Roche, BMC9318, #1170376001, 1:50), overnight at 4°C. Following three washes with PBS-PVA, parthenotes were incubated with solution containing Alexa-Fluor-labeled secondary antibodies (Invitrogen), and DNA was counterstained with DAPI. Finally, samples were washed three times with PBS-PVA and mounted using Vectashield.

Immunoblotting

Samples were lysed in NuPAGE sample buffer (Invitrogen) at 70°C for 10 min, loaded onto NuPAGE™ 4-12% Bis-Tris gel, separated in MOPS or 2-(N-morpholino)ethanesulfonic acid (MES) buffer, and blotted onto an Immobilon-P transfer membrane (Millipore). After blocking with 10% non-fat dry milk in 1×TBS containing 0.1% polysorbate 20, membranes were probed with α-tubulin (Sigma, DM1A, #T9026, 1:2500−1:10,000), GFP (Nacalai Tesque, 1:1000), CREST (1:5000 −1:10,000) and NPM2 (1:5000). Primary antibodies were detected with appropriate secondary antibodies conjugated with HRP (Jackson Immunoresearch) followed by detection using a Chemi-Lumi One Super (Nacalai) or SuperSignal West Femto detection system (Thermo Fisher Scientific).

Culture of HEK293T cells and transfection

HEK293T cells were cultured in DMEM culture medium (Invitrogen) supplemented with 10% fetal calf serum and 8 µg/ml kanamycin. Cells at the concentration of 2.0×10^5 were seeded in a six-well dish, cultured for 24 h and transfected with 3 µg plasmid DNA using Lipofectamine 2000 (Invitrogen) according to manufacturer's instructions. Following 24 h of transfection, the transfected cells were extracted with sample buffer for immunoblot analysis.

Transmission electron microscopy

Samples were fixed by 4% paraformaldehyde and 2% glutaraldehyde overnight at 4°C. After several washes with PBS, samples were embedded in 3% agarose-PBS. They were then post-fixed using 2% OsO_4 in 100 mM phosphate buffer for 2 h at room temperature, dehydrated in a series of graded ethanol solutions, embedded in epoxy resin and polymerized at 60°C for 3 days. Tissue samples were cut into ultra-thin sections (70 nm) on an ultramicrotome EM UC6 (Leica). Following staining with uranyl acetate and lead citrate staining solution (Sigma), the ultra-thin sections were viewed under an H-7650 transmission electron microscope (Hitachi-Hightech).

Acknowledgements

We thank Fugaku Aoki for the *Npm2*-truncation mutant plasmids, Jibak Lee for the pCS2 and pCS2-*eGfp* plasmids, Takaya Abe and Toshihiko Fujimori for the pcDNA3-*H2b-mCherry* plasmid, Yoshinao Muro for CREST serum, Kaori Yamanaka and Fumiaki Itoi for their assistance in live-cell imaging, Koji Nagao for MS analysis, and Bungo Akiyoshi, Takayuki Hirota and members of the Saitou and Nasmyth labs for their critical input. We are immensely indebted to Akira Nakamura for guidance with the molecular biological procedures and to Jonathan Godwin and Kim Nasmyth for their kind support of revision experiments.

Competing interests

The authors declare no competing or financial interests.

Author contributions

Conceptualization: S.O.; Methodology: S.O., K.Y., C.O., K.F.; Validation: S.O., K.Y.; Formal analysis: S.O., C.O.; Investigation: S.O., K.Y., C.O., K.F.; Resources: S.O., K.Y., C.O., K.F., T.W., M.M.M.; Data curation: C.O.; Writing - original draft: S.O.; Writing - review & editing: M.M.M., M.S.; Visualization: S.O.; Supervision: C.O., T.W., M.M.M., M.S.; Project administration: S.O., M.S.; Funding acquisition: S.O.

Funding

This work was supported in part by a Grant-in-Aid from Ministry of Education, Culture, Sports, Science, and Technology (MEXT) to S.O. and by funds from the Hakubi Center for Advanced Research (to S.O.). Support for the generation of *Npm2*-knockout mice and anti-NPM2 antibody were provided by a grant from Eunice Kennedy Shriver National Institute of Child Health and Human Development (NICHD) (grant number. R01-HD33438 to M.M.M.).

Data availability

Supplementary information

Supplementary information available online at
http://jcs.biologists.org/lookup/doi/10.1242/jcs.195875.supplemental

References

Amin, M. A., Matsunaga, S., Uchiyama, S. and Fukui, K. (2008). Nucleophosmin is required for chromosome congression, proper mitotic spindle formation, and kinetochore-microtubule attachment in HeLa cells. *FEBS Lett.* **582**, 3839-3844.

Aoki, F., Worrad, D. M. and Schultz, R. M. (1997). Regulation of transcriptional activity during the first and second cell cycles in the preimplantation mouse embryo. *Dev. Biol.* **181**, 296-307.

Arney, K. L., Bao, S., Bannister, A. J., Kouzarides, T. and Surani, M. A. (2002). Histone methylation defines epigenetic asymmetry in the mouse zygote. *Int. J. Dev. Biol.* **46**, 317-320.

Banani, S. F., Lee, H. O., Hyman, A. A. and Rosen, M. K. (2017). Biomolecular condensates: organizers of cellular biochemistry. *Nat. Rev. Mol. Cell Biol.* **18**, 285-298.

Bergeron-Sandoval, L.-P., Safaee, N. and Michnick, S. W. (2016). Mechanisms and consequences of macromolecular phase separation. *Cell* **165**, 1067-1079.

Brangwynne, C. P. (2013). Phase transitions and size scaling of membrane-less organelles. *J. Cell Biol.* **203**, 875-881.

Broccoli, D., Miller, O. J. and Miller, D. A. (1990). Relationship of mouse minor satellite DNA to centromere activity. *Cytogenet. Cell Genet.* **54**, 182-186.

Burns, K. H., Viveiros, M. M., Ren, Y., Wang, P., DeMayo, F. J., Frail, D. E., Eppig, J. J. and Matzuk, M. M. (2003). Roles of NPM2 in chromatin and nucleolar organization in oocytes and embryos. *Science* **300**, 633-636.

Chatot, C. L., Ziomek, C. A., Bavister, B. D., Lewis, J. L. and Torres, I. (1989). An improved culture medium supports development of random-bred 1-cell mouse embryos in vitro. *J. Reprod. Fertil.* **86**, 679-688.

Chouinard, L. A. (1971). A light- and electron-microscope study of the nucleolus during growth of the oocyte in the prepubertal mouse. *J. Cell Sci.* **9**, 637-663.

Colombo, E., Alcalay, M. and Pelicci, P. G. (2011). Nucleophosmin and its complex network: a possible therapeutic target in hematological diseases. *Oncogene* **30**, 2595-2609.

Dunleavy, E. M., Roche, D., Tagami, H., Lacoste, N., Ray-Gallet, D., Nakamura, Y., Daigo, Y., Nakatani, Y. and Almouzni-Pettinotti, G. (2009). HJURP Is a cell-cycle-dependent maintenance and deposition factor of CENP-A at centromeres. *Cell* **137**, 485-497.

Feric, M., Vaidya, N., Harmon, T. S., Mitrea, D. M., Zhu, L., Richardson, T. M., Kriwacki, R. W., Pappu, R. V. and Brangwynne, C. P. (2016). Coexisting liquid phases underlie nucleolar subcompartments. *Cell* **165**, 1686-1697.

Foltz, D. R., Jansen, L. E. T., Bailey, A. O., Yates, J. R., Bassett, E. A., Wood, S., Black, B. E. and Cleveland, D. W. (2009). Centromere-specific assembly of CENP-A nucleosomes is mediated by HJURP. *Cell* **137**, 472-484.

Fukagawa, T. and Earnshaw, W. C. (2014). The centromere: chromatin foundation for the kinetochore machinery. *Dev. Cell* **30**, 496-508.

Fulka, H. and Fulka, J. (2007). The use of micromanipulation methods as a tool to prevention of transmission of mutated mitochondrial DNA. *Curr. Top. Dev. Biol.* **77**, 187-211.

Fulka, H. and Langerova, A. (2014). The maternal nucleolus plays a key role in centromere satellite maintenance during the oocyte to embryo transition. *Development* **141**, 1694-1704.

Fulka, J., Jr, Moor, R. M., Loi, P. and Fulka, J. (2003). Enucleolation of porcine oocytes. *Theriogenology* **59**, 1879-1885.

Geuskens, M. and Alexandre, H. (1984). Ultrastructural and autoradiographic studies of nucleolar development and rDNA transcription in preimplantation mouse embryos. *Cell Differ.* **14**, 125-134.

Hao, L., Vassena, R., Wu, G., Han, Z., Cheng, Y., Latham, K. E. and Sapienza, C. (2009). The unfolded protein response contributes to preimplantation mouse embryo death in the DDK syndrome. *Biol. Reprod.* **80**, 944-953.

Hayashi-Takanaka, Y., Yamagata, K., Nozaki, N. and Kimura, H. (2009). Visualizing histone modifications in living cells: Spatiotemporal dynamics of H3 phosphorylation during interphase. *J. Cell Biol.* **187**, 781-790.

Holmberg Olausson, K., Nistér, M. and Lindström, M. S. (2014). Loss of nucleolar histone chaperone NPM1 triggers rearrangement of heterochromatin and synergizes with a deficiency in DNA methyltransferase DNMT3A to drive ribosomal DNA transcription. *J. Biol. Chem.* **289**, 34601-34619.

House, N. C. M., Koch, M. R. and Freudenreich, C. H. (2014). Chromatin modifications and DNA repair: Beyond double-strand breaks. *Front. Genet.* **5**, 296.

Inoue, A. and Aoki, F. (2010). Role of the nucleoplasmin 2 C-terminal domain in the formation of nucleolus-like bodies in mouse oocytes. *FASEB J.* **24**, 485-494.
Inoue, A. and Zhang, Y. (2014). Nucleosome assembly is required for nuclear pore complex assembly in mouse zygotes. *Nat. Struct. Mol. Biol.* **21**, 609-616.
Inoue, A., Ogushi, S., Saitou, M., Suzuki, M. G. and Aoki, F. (2011). Involvement of mouse nucleoplasmin 2 in the decondensation of sperm chromatin after fertilization. *Biol. Reprod.* **85**, 70-77.
Kleinschmidt, J. A., Fortkamp, E., Krohne, G., Zentgraf, H. and Franke, W. W. (1985). Co-existence of two different types of soluble histone complexes in nuclei of Xenopus laevis oocytes. *J. Biol. Chem.* **260**, 1166-1176.
Kyogoku, H., Fulka, J., Jr, Wakayama, T. and Miyano, T. (2014). De novo formation of nucleoli in developing mouse embryos originating from enucleolated zygotes. *Development* **141**, 2255-2259.
Laskey, R. A., Honda, B. M., Mills, A. D. and Finch, J. T. (1978). Nucleosomes are assembled by an acidic protein which binds histones and transfers them to DNA. *Nature* **275**, 416-420.
Liu, J.-L., Buszczak, M. and Gall, J. G. (2006). Nuclear bodies in the Drosophila germinal vesicle. *Chromosom. Res.* **14**, 465-475.
Mitrea, D. M., Cika, J. A., Guy, C. S., Ban, D., Banerjee, P. R., Stanley, C. B., Nourse, A., Deniz, A. A. and Kriwacki, R. W. (2016). Nucleophosmin integrates within the nucleolus via multi-modal interactions with proteins displaying R-rich linear motifs and rRNA. *Elife* **5**, e13571.
Nozawa, R.-S., Nagao, K., Masuda, H.-T., Iwasaki, O., Hirota, T., Nozaki, N., Kimura, H. and Obuse, C. (2010). Human POGZ modulates dissociation of HP1alpha from mitotic chromosome arms through Aurora B activation. *Nat. Cell Biol.* **12**, 719-727.
Ogushi, S. and Saitou, M. (2010). The nucleolus in the mouse oocyte is required for the early step of both female and male pronucleus organization. *J. Reprod. Dev.* **56**, 495-501.
Ogushi, S., Palmieri, C., Fulka, H., Saitou, M., Miyano, T. and Fulka, J. (2008). The maternal nucleolus is essential for early embryonic development in mammals. *Science* **319**, 613-616.
Ohsumi, K. and Katagiri, C. (1991). Characterization of the ooplasmic factor inducing decondensation of and protamine removal from toad sperm nuclei: Involvement of nucleoplasmin. *Dev. Biol.* **148**, 295-305.
Okuwaki, M., Matsumoto, K., Tsujimoto, M. and Nagata, K. (2001). Function of nucleophosmin/B23, a nucleolar acidic protein, as a histone chaperone. *FEBS Lett.* **506**, 272-276.
Padeken, J., Mendiburo, M. J., Chlamydas, S., Schwarz, H.-J., Kremmer, E. and Heun, P. (2013). The nucleoplasmin homolog NLP mediates centromere clustering and anchoring to the nucleolus. *Mol. Cell* **50**, 236-249.
Philpott, A. and Leno, G. H. (1992). Nucleoplasmin remodels sperm chromatin in Xenopus egg extracts. *Cell* **69**, 759-767.
Philpott, A., Leno, G. H. and Laskey, R. A. (1991). Sperm decondensation in Xenopus egg cytoplasm is mediated by nucleoplasmin. *Cell* **65**, 569-578.
Platonova, O., Akey, I. V., Head, J. F. and Akey, C. W. (2011). Crystal structure and function of human nucleoplasmin (Npm2): a histone chaperone in oocytes and embryos. *Biochemistry* **50**, 8078-8089.
Probst, A. V., Santos, F., Reik, W., Almouzni, G. and Dean, W. (2007). Structural differences in centromeric heterochromatin are spatially reconciled on fertilisation in the mouse zygote. *Chromosoma* **116**, 403-415.
Probst, A. V., Okamoto, I., Casanova, M., El Marjou, F., Le Baccon, P. and Almouzni, G. (2010). A Strand-specific burst in transcription of pericentric satellites is required for chromocenter formation and early mouse development. *Dev. Cell* **19**, 625-638.
Quinn, P., Kerin, J. F. and Warnes, G. M. (1985). Improved pregnancy rate in human in vitro fertilization with the use of a medium based on the composition of human tubal fluid. *Fertil. Steril.* **44**, 493-498.
Saitou, M., Kagiwada, S. and Kurimoto, K. (2012). Epigenetic reprogramming in mouse pre-implantation development and primordial germ cells. *Development* **139**, 15-31.
Shin, Y., Berry, J., Pannucci, N., Haataja, M. P., Toettcher, J. E. and Brangwynne, C. P. (2017). Spatiotemporal control of intracellular phase transitions using light-activated optoDroplets. *Cell* **168**, 159-171.e14.
Shishova, K. V., Lavrentyeva, E. A., Dobrucki, J. W. and Zatsepina, O. V. (2015). Nucleolus-like bodies of fully-grown mouse oocytes contain key nucleolar proteins but are impoverished for rRNA. *Dev. Biol.* **397**, 267-281.
Sutovsky, P. and Schatten, G. (1998). Ultrastructural aspects of mammalian fertilization: new discoveries and inspirations from the work of Daniel Szöllösi. *Reprod. Nutr. Dev.* **38**, 629-641.
Tjong, H., Li, W., Kalhor, R., Dai, C., Hao, S., Gong, K., Zhou, Y., Li, H., Zhou, X. J., Le Gros, M. A. et al. (2016). Population-based 3D genome structure analysis reveals driving forces in spatial genome organization. *Proc. Natl. Acad. Sci. USA* **113**, E1663-E1672.
Voon, H. P. J. and Wong, L. H. (2016). New players in heterochromatin silencing: histone variant H3.3 and the ATRX/DAXX chaperone. *Nucleic Acids Res.* **44**, 1496-1501.
Wijchers, P. J., Geeven, G., Eyres, M., Bergsma, A. J., Janssen, M., Verstegen, M., Zhu, Y., Schell, Y., Vermeulen, C., de Wit, E. et al. (2015). Characterization and dynamics of pericentromere-associated domains in mice. *Genome Res.* **25**, 958-969.
Zatsepina, O. V., Bouniol-Baly, C., Amirand, C. and Debey, P. (2000). Functional and molecular reorganization of the nucleolar apparatus in maturing mouse oocytes. *Dev. Biol.* **223**, 354-370.

Figure S1

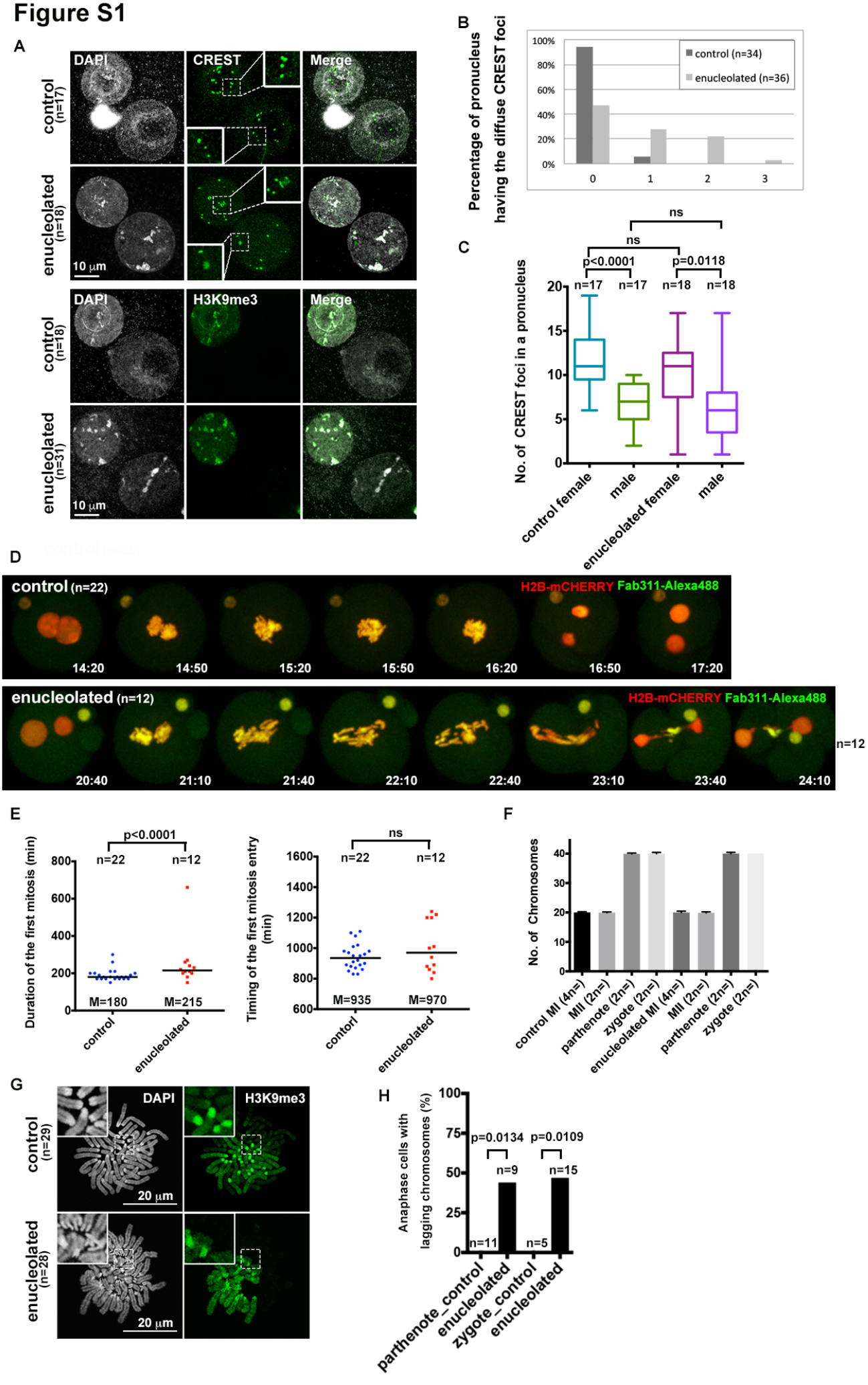

Figure S1

Loss of the oocyte nucleolus caused disorganization of higher chromatin in pronuclei and chromosome mis-segregation during the first mitosis in zygotes.

(A) Immunostaining using zygotes from enucleolated oocytes with the antibodies (green) shown in the panels. Insets show the diffuse CREST signals (>2 μm^2) in each pronucleus at 2-fold magnification. DNA was stained with DAPI (grey). Control, zygotes from nucleolus-reinjected oocytes. (B) Percentage of pronuclei having diffuse CREST signals in zygotes from control/enucleolated oocytes. The numbers on the x-axis of the graph indicate the number of diffuse signals in each pronucleus. (C) The number of CREST foci in each pronucleus of zygotes from control/enucleolated oocytes. The boxes show the median, 25th, and 75th percentiles, and the bars show the 10th and 90th percentiles. Two-tailed Mann-Whitney test. ns, not significant. (D) Representative stills from live cell imaging of zygotes from control/enucleolated oocytes. Chromosomes were labeled by H2B-mCHERRY (red) and chromosome condensation was visualized by Fab311-Alexa488 (green). The numbers in each panel show the time after sperm injection (hr:min). (E) The duration and entry timing of the first mitosis in zygotes are plotted. The numbers of zygotes measured in three independent experiments are indicated above the plots. Bars, median (M). Two-tailed Mann-Whitney test. (F) Representative images of chromosome spreads in zygotes stained with H3K9me3 antibody (green) and DAPI (grey). Insets in each panel are 2.5-fold magnifications of the regions shown in the dash-lined boxes. (G) The number of chromosomes in first meiosis (MI), second meiosis (MII), and parthenotes/zygotes from control/enucleolated oocytes. (n>10) Bars, SD. (H) The incidence rate of chromosome lagging during the first anaphase in parthenotes/zygotes from enucleolated oocytes. Two-tailed Chi-square test. (A-G, H) n, the numbers of parthenotes/zygotes measured in three independent experiments.

Figure S2

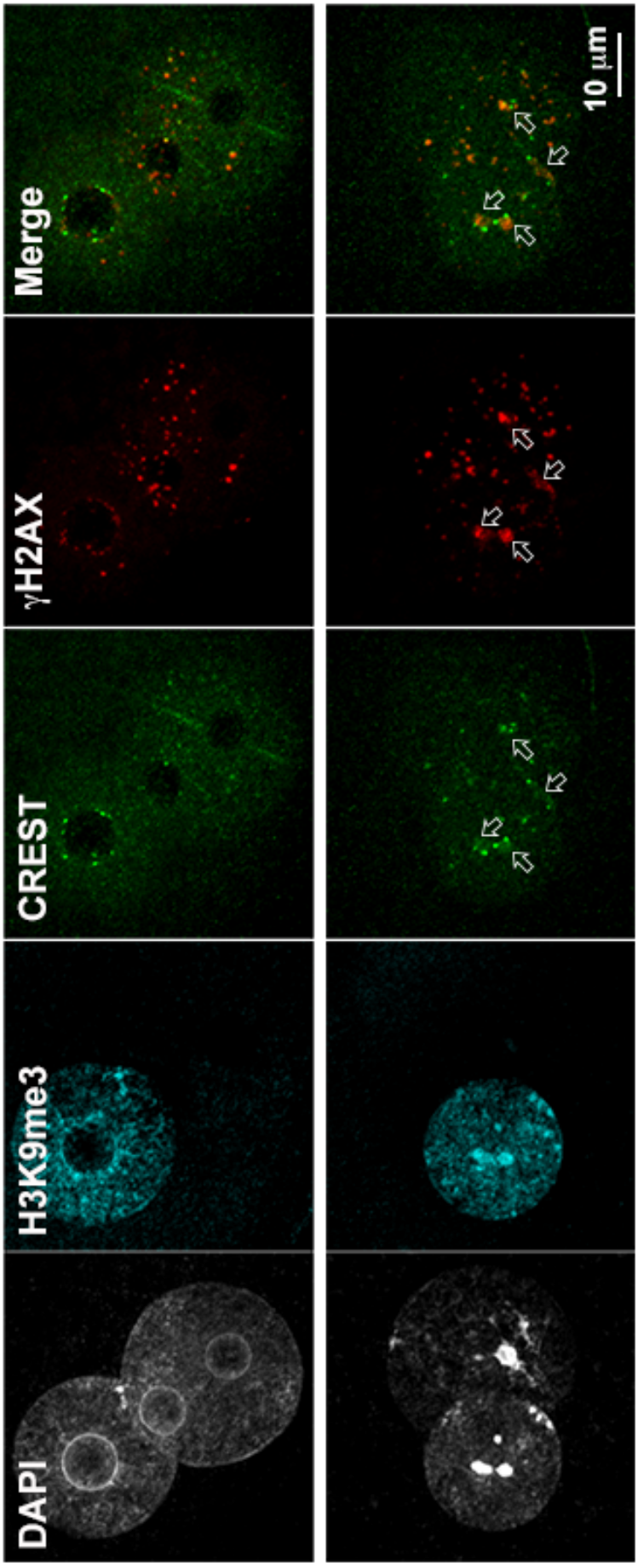

Figure S2

Loss of the oocyte nucleolus caused DNA damage especially at the diffused CREST signals of pronuclei in zygotes.

Immunostaining using zygotes from enucleolated oocytes 12 hr after fertilization with the antibodies shown in the panels. Arrows indicate the regions positive for γ-H2AX and diffused CREST signals. (control: n= 8, enucleolated: n=11)

Figure S3

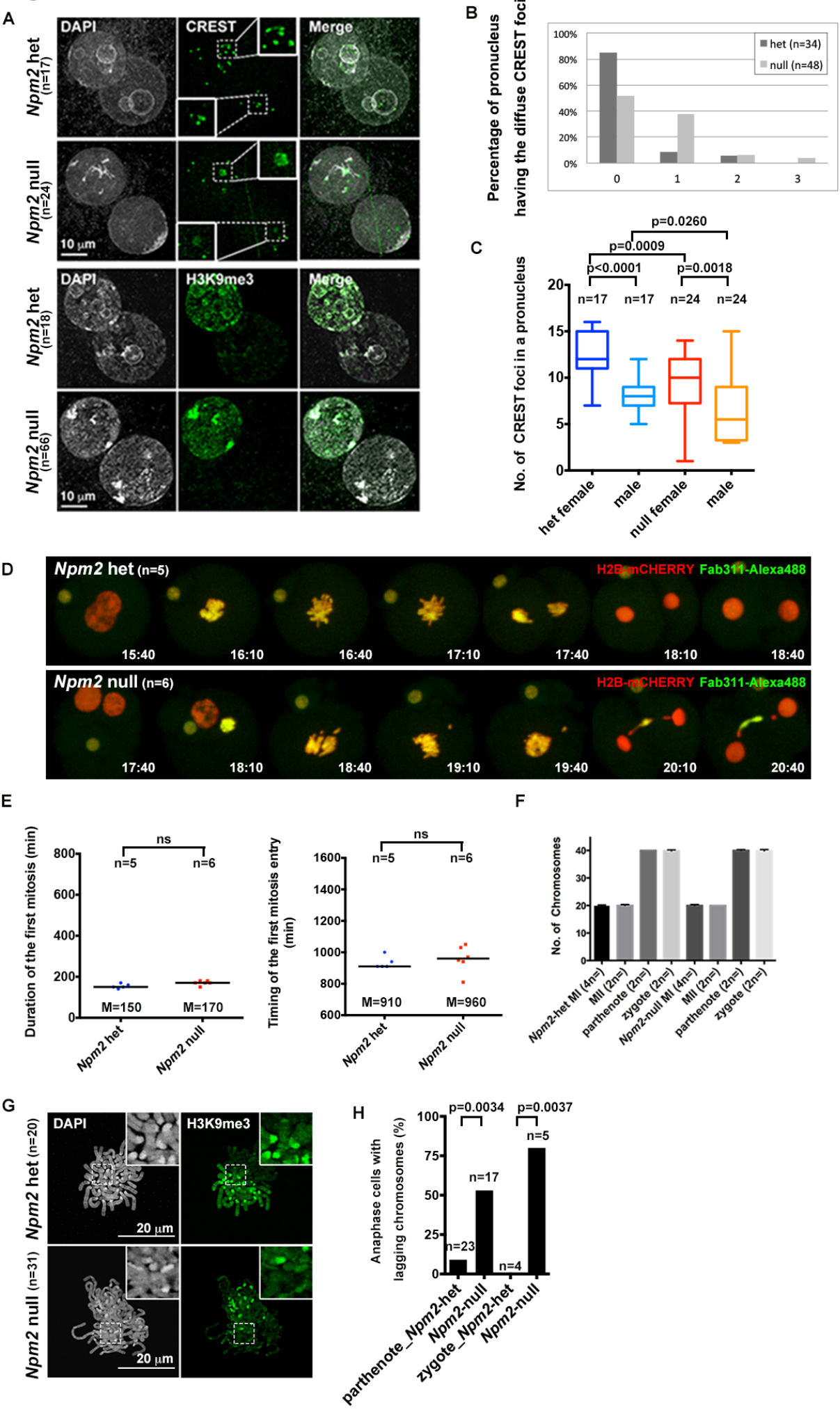

Figure S3

Zygotes from *Npm2*-null oocytes also showed defects in higher-chromatin organization in pronuclei and chromosome mis-segregation during the first mitosis.

(A) Zygotes from *Npm2*-null oocytes stained with the antibodies shown in the panels (green) and with DAPI (grey). Insets show the diffuse CREST signals at 2-fold magnification. (B) Percentage of pronuclei having diffuse CREST signals in zygotes from *Npm2*-het/-null oocytes. (C) The number of CREST foci in each pronucleus of zygotes from *Npm2*-het/-null oocytes. Two-tailed Mann-Whitney test. ns, not significant. (D) Representative stills from live cell imaging of zygotes according to the method shown in Figure S1D. (E) Plots of the duration and entry timing of the first mitosis in zygotes. The numbers of zygotes measured in three independent experiments are indicated above the plots. Bars, median (M). Two-tailed Mann-Whitney test. (F) Representative images of chromosome spreads in zygotes stained with H3K9me3 antibody (green) and with DAPI (grey). Insets in each panel are 2.5-fold magnifications. (G) The number of chromosomes in first meiosis (MI), second meiosis (MII), and parthenotes/zygotes from *Npm2*-het/-null oocytes. (n>10) Bars, SD. (H) The incidence rate of chromosome lagging during the first anaphase in parthenotes/zygotes from *Npm2*-het/-null oocytes. Two-tailed Chi-square test. (A-G, H) n, the numbers of parthenotes/zygotes measured in three independent experiments.

Figure S4

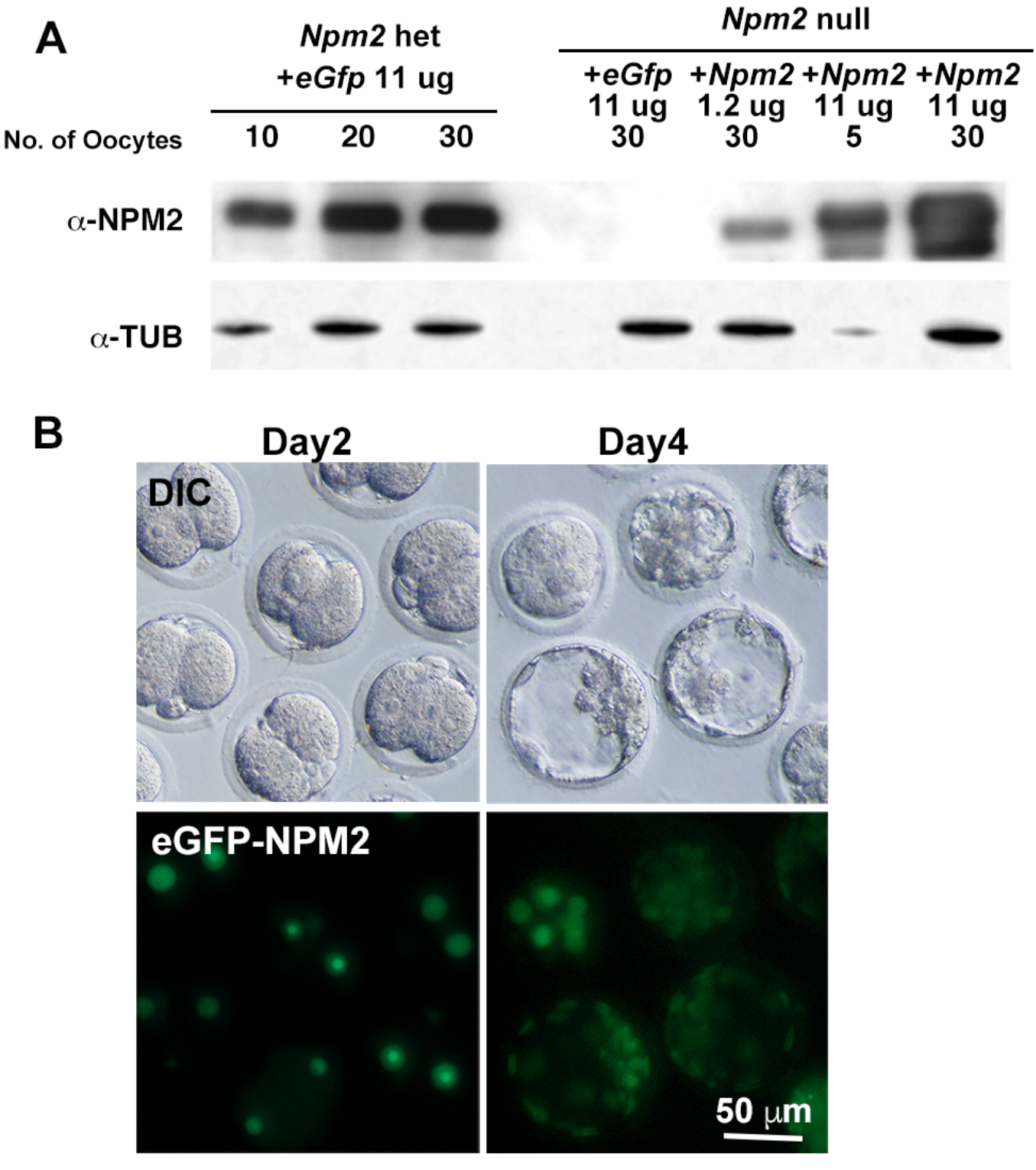

Figure S4

The early embryonic development of embryos from *Npm2*-null oocytes was rescued by NPM2 in a concentration-dependent manner.

(A) NPM2 protein expression level in *Npm2*-null oocytes rescued by various concentrations of *Npm2*-mRNAs. The oocyte number in each sample is indicated above the blots and alpha-TUBULIN (TUB) was used as a loading control (n=3). (B) *eGfp-Npm2* mRNA injected into MII oocytes was expressed through to the blastocyst stage. DIC, differential interference contrast.

Figure S5

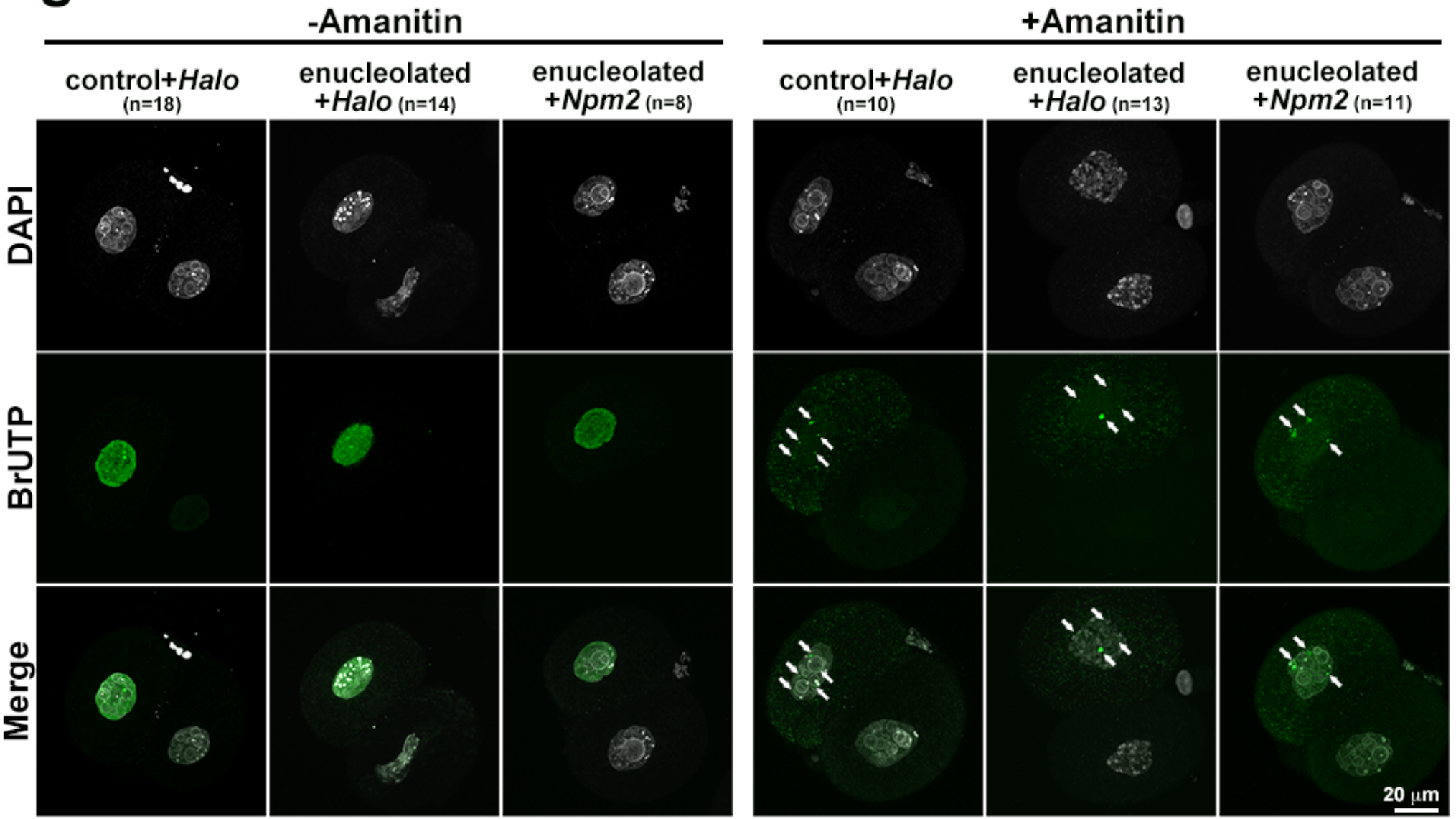

J. Cell Sci. 130: doi:10.1242/jcs.195875: Supplementary information

Figure S5

Late 2-cell embryos from enucleolated oocytes resumed nascent transcription of total RNA and r RNA.

Immunostaining using parthenotes from enucleolated oocytes and from enucleolated oocytes injected with *Npm2* mRNA 38-40 hr after artificial activation with the antibodies shown in the panels. The panels under –Amanitin shows nascent transcripts of total RNA, and those under +Amanitin shows nascent transcripts of rRNA (arrows). n, the numbers of embryos measured in two independent experiments.

J. Cell Sci. 130: doi:10.1242/jcs.195875: Supplementary information

Figure S6

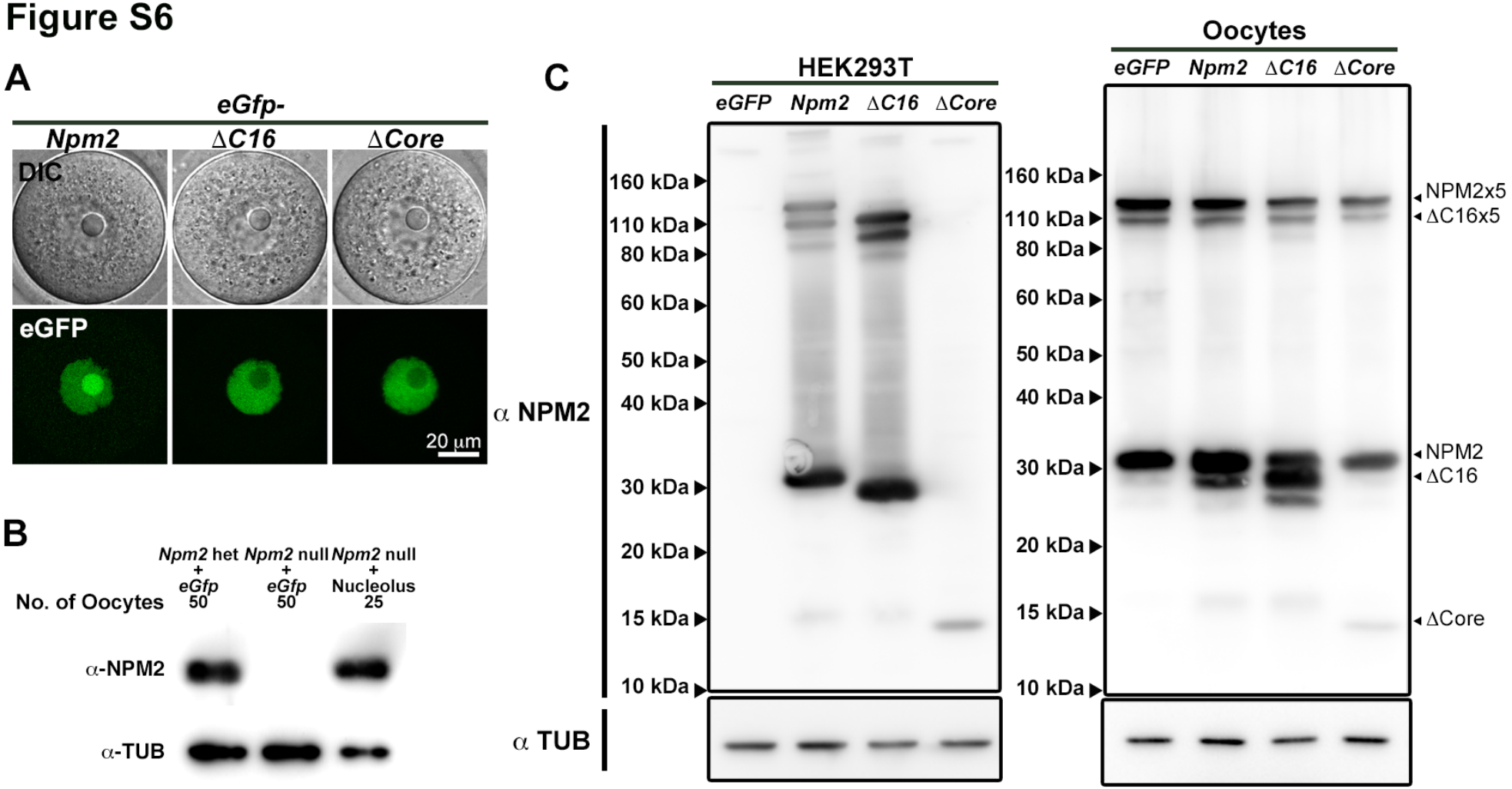

Figure S6

Expression of NPM2 truncation mutants disrupted pentamer formation of endogenous NPM2

(A) Localization of NPM2 truncated mutants in oocytes at the germinal vesicle stage. DIC, differential interference contrast. (B) NPM2 protein expression level in *Npm2*-het oocytes. Half of *Npm2*-null oocytes injected with nucleoli from wild oocytes showed a level of NPM2 expression similar to that of *Npm2*-het oocytes. The oocyte number in each sample is indicated above the blots and TUB was used as a loading control (n=3). (C) NPM2 truncation mutants were expressed in HEK293T cells transiently, and in oocytes by mRNA injection. Each lane was loaded with 5 μg of total proteins from each group that expressed the indicated plasmids in HEK293T cells or 40 oocytes injected with the indicated mRNAs. The oocyte number in each sample is indicated above the blots and TUB was used as a loading control (n=3).

Table S1. The average duration and entry timing of the first mitosis in parthenotes/zygotes from control/enucleolated and *Npm2*-het/-null oocytes

Experimental Group	Average Duration of 1stM (mean±SD)	Average Timing of 1stM Entry (mean±SD)
control Sr^{2+}	176.6±43.04[a]	932.9±73.95[a]
enucleolated Sr^{2+}	235.6±90.76[b]	1085±195.3[b]
Npm2-het Sr^{2+}	183.3±38.46[a]	865.0±30.00[a]
Npm2-null Sr^{2+}	192.5±46.34[a]	897.5±47.31[a]
control ICSI	190.9±33.08[a]	942.7±83.11[a]
enucleolated ICSI	252.5±132.5[b]	1007±165.4[a]
Npm2-het ICSI	154.0±11.40[a]	934.0±39.12[a]
Npm2-null ICSI	170.0±10.95[a]	958.3±84.95[a]

Values with different superscript within the same line are significantly different by two-tailed Mann-Whitney test ($p<0.05$).

Table S2. The list of proteins identified from nucleoli isolated from mouse GV-oocytes

Click here to Download Table S2

Table S3. Developmental potency of embryos from *Npm2*-het/-null oocytes injected with *Npm2* truncated mutant mRNAs

		eGfp	*Npm2*	*ΔC16*
		11 μg/μl	11μg/μl	11μg/μl
Npm2 het	No of Embryos Transferred	40	40	40
	No of Pups Obtained	18[a]	21[a]	0
Npm2 null	No of Embryos Transferred	42	61	38
	No of Pups Obtained	0	33[a]	0

Values with different superscript within the same raw are significantly different by chi-square test ($p<0.05$).